Toward multiloop local renormalization within causal loop-tree duality

José Ríos-Sánchez[1] and German Sborlini[1,2]

[1]*Departamento de Física Fundamental e IUFFyM, Universidad de Salamanca, Plaza de la Merced S/N, 37008 Salamanca, Spain*

[2]*GFIMA—Escuela de Ciencias, Ingeniería y Diseño, Universidad Europea de Valencia, Paseo de la Alameda 7, 46010 Valencia, Spain*

(Received 26 February 2024; accepted 8 May 2024; published 3 June 2024)

Renormalization is a well-known technique to get rid of ultraviolet (UV) singularities. When relying on dimensional regularization, these become manifest as ϵ poles, allowing one to define counterterms with useful recursive properties. However, this procedure requires one to work at "integral level" and poses difficulties to achieve a smooth combination with seminumerical approaches. This article is devoted to the development of an integrand-level renormalization formalism, better suited for semi- or fully numerical calculations. Starting from the loop-tree duality, we keep the causal representations of the integrands of multiloop Feynman diagrams and explore their UV behavior. Then, we propose a strategy that allows one to build local counterterms, capable of rendering the expressions integrable in the high-energy limit and in four space-time dimensions. Our procedure was tested on diagrams up to three loops, and we found a remarkably smooth cancellation of divergences. The results of this work constitute a powerful step toward a fully local renormalization framework in quantum field theory.

DOI: 10.1103/PhysRevD.109.125004

I. INTRODUCTION AND MOTIVATION

In the quest for precision in high-energy physics, the need to compute higher perturbative orders has become essential. Current and future high-energy colliders will collect an enormous amount of data, which will lead to very precise measurements. From the theory side, this translates into a huge challenge to reduce the uncertainties in the predictions extracted from quantum field theories (QFTs) and pushes the available computational frameworks to their limits.

In spite of the recent developments of several new methodologies to tackle higher-order calculations [1], there are some bottlenecks reluctant to be solved. One of them is related to the presence of divergences and their nonlocal cancellation. It is well known that generic QFTs possess singularities in the high-energy limit, the so-called ultraviolet (UV) divergences. For the particular case of gauge theories, it is also known [2,3] that these divergences can be always absorbed or hidden within free parameters of the theory, through the renormalization procedure. On the other hand, QFTs with massless particles also have low-energy divergences, known as infrared (IR) singularities. As in the UV case, there are several well-established methods to tackle them, which mostly consist of adding and removing suitable counterterms [4].

Both for IR and UV singularities, it is required to introduce a regularization prescription to make manifest and handle the divergences. Because of its nice properties, dimensional regularization (DREG) [2,5–7] has become a rather standard approach. When working with $D = 4 - 2\epsilon$ space-time dimensions, the singularities manifest as poles in ϵ. In the IR sector, the ϵ poles cancel when we consider IR-safe observables and we put together all the degenerated configurations that include extra real radiation and virtual particles [8]. Within the traditional subtraction approaches, this cancellation occurs *after* integration of the real radiation and loop amplitudes, including some suitable counterterms. Analogously, the UV divergences are removed through renormalization counterterms, which include ϵ poles that exactly match those present in the virtual amplitudes. At this point, we have to emphasize that UV divergences are only originated inside the loops, due to the fact that the energy of the virtual states is unconstrained.

The computational framework described before has been successfully applied to several relevant processes in collider physics, up to next-to-next-to-leading order, which has become the "new standard" in precision. Very recently, next-to-next-to-next-to-leading order results appeared [9], although the effort required to achieve them is increasing enormously when adding extra loops or legs. Among the different bottlenecks, there are severe difficulties to analytically calculate multiloop, multileg Feynman integrals within DREG, since the presence of IR and UV singularities

prevents a straightforward numerical implementation. Additionally, IR divergences within loops avoid a direct numerical cancellation with those present in the real-emission contributions, forcing one to use nonlocal or semi-analytical techniques to render the expressions IR finite.

With this panorama in mind, novel techniques to explore an efficient point-by-point or local cancellation of singularities *before* integration are required [10–13]. In this direction, the loop-tree duality (LTD) [14–23] allows one to open loop amplitudes into sums of tree-level-like objects integrated over a phase space, closely resembling the real-radiation contribution. Using this formalism, the IR singular structure of the loops is expressed in terms of phase-space integrals [17], suggesting a clear connection to the real-radiation contribution. In fact, this constitutes the basis of the four-dimensional unsubtraction (FDU) framework [24–27], where the "open loops" or dual amplitudes are combined with the real radiation by means of suitable momentum mappings. As a result, FDU provides integrand-level expressions that are explicitly free of IR singularities, which are canceled locally (i.e., point-by-point) integration, rendering the expression not only finite, but also (and most importantly) integrable.

In order to achieve a local cancellation of UV divergences, there are some recent methodologies in the market [28–33], although most of them are not optimized for local IR counterterms. Within the FDU framework, the treatment of UV singularities is slightly different, but the objective is the same: develop local renormalization counterterms. Even if the well-known Bogoliubov-Parasiuk-Hepp-Zimmermann (BPHZ) renormalization program [34–43] provides a systematic way of computing local UV subtraction counterterms, it was mainly thought for renormalization in Minkowski space and requires some adjustments to be incorporated within the FDU framework. Our procedure is inspired in the expansion around UV propagators [44–47], combined with the application of the LTD and a suitable matching procedure to recover results in DREG-defined schemes (such as $\overline{\text{MS}}$). In this way, FDU has proven able to achieve a fully local cancellation of both IR and UV divergences up to next-to-leading order (NLO). Still, local UV renormalization in FDU beyond NLO is an open problem. A strategy to deal with UV singularities up to two-loop level was developed in Refs. [45,47], allowing to numerically reproduce some well-known $\overline{\text{MS}}$ results.

In this article, we explore a LTD-based strategy that makes use of the so-called causal representation [48–57] to unveil local UV counterterms for multiloop Feynman integrals. The methodology is inspired, again, in the expansion around UV propagators, but acting directly on the Euclidean space of the causal dual integrands (i.e., the integrands of the Feynman amplitudes after the application of the manifestly causal LTD). We used the fact that the causal dual representation has an analogous structure to the real-radiation phase space, allowing us to split the integrand in such a way that we can isolate the UV-divergent contributions more efficiently.

The outline of this article is the following. In Sec. II, we briefly review the basis of manifestly causal LTD and its mathematical properties. Then, we discuss the generation of local UV counterterms in Sec. III. We start reviewing in Sec. III A the strategy presented in Refs. [45,46], and we explain the causal-inspired approach in Sec. III B. After presenting the general formalism, we explore useful simplifications to keep the causal structure in the local counterterms in Sec. III C. In Sec. IV, we apply our renormalization methodology to two- and three-loop representative diagrams, showing a smooth convergence in the UV region. After discussing the results within our method, we provide a comparison with the BPHZ renormalization program in Sec. V, highlighting the similarities and differences. Also, we include in the Appendix an analysis about the momentum expansions leading to the UV counterterms in both approaches. Finally, we present the conclusions and future research directions in Sec. VI.

II. CAUSAL LOOP-TREE DUALITY

The motivation behind the LTD is intuitive: open loop diagrams into a collection of tree-level-like objects. To achieve this purpose, we make use of Cauchy's residue theorem to remove 1 degree of freedom per loop. In particular, we choose to integrate out the energy component of each loop momenta, which transforms the integration domain from Minkowski to Euclidean space. This point is very important in order to reach an integrand-level combination of the different ingredients involved in higher-order cross section computations (namely, the real radiation and the virtual corrections). Furthermore, integrating out the energy component implies putting on shell certain internal lines of the diagrams.

In its original form, LTD decomposes any one- and two-loop scattering amplitude in any QFT into a sum of trees where some subsets of propagators were replaced by the so-called "dual propagators" [14–16,58]. The dual propagators, denoted $G_D(q_i;q_j)$, have a momentum-dependent prescription that allows one to capture all the information contained in the multiple cuts originated from the Feynman tree theorem [59]. The integrand obtained after the application of the LTD is called the dual integrand or dual representation of the associated Feynman integral or multiloop scattering amplitude.

Recently, it was found that the iterated application of the Cauchy residue theorem directly leads to the dual representation. To illustrate this, let us consider a generic L-loop scattering amplitude with N external particles,

$$\begin{aligned}\mathcal{A}_N^{(L)} &= \int_{\ell_1\ldots\ell_L} \sum_j \mathcal{N}_j \times G_F(1,\ldots,L,\ldots,n) \\ &\approx \int_{\ell_1\ldots\ell_L} d\mathcal{A}_N^{(L)}(1,\ldots,n), \end{aligned} \tag{1}$$

where $\mathcal{N}$ corresponds to the numerator (depending on the loop and external momenta, $\{\ell_i\}_{i=1,\ldots,L}$ and $\{p_i\}_{i=1,\ldots,N}$, respectively), and $G_F(1,\ldots,L,\ldots,n)$ denotes a product of Feynman propagators associated with the underlying topology. $\{1,\ldots,n\}$ denotes sets of internal momenta that depend on specific combinations of loop momenta. For the sake of simplicity, we can assume 1 depends only on ℓ_1, 2 only on ℓ_2, and so on, while the remaining are nontrivial linear combinations of $\{\ell_i\}_{i=1,\ldots,L}$. Regarding the integration measure, we have

$$\int_{\ell_1\ldots\ell_L} = (-i\mu^{4-d})^L \int \frac{d^d\ell_1}{(2\pi)^d}\cdots\frac{d^d\ell_L}{(2\pi)^d}, \tag{2}$$

which is valid for an arbitrary number of space-time dimensions d, and μ denotes an energy scale associated with the regularization procedure (DREG in this case).

We start by taking the residue over the energy component of ℓ_1, which is equivalent to put on shell, one by one, the propagators of 1, i.e.,

$$\mathcal{A}_D^{(L)}(1;2,\ldots,n) = \sum_{i_1\in 1}\mathrm{Res}\Big(d\mathcal{A}_N^{(L)}(1,\ldots,n);q_{i_1,0}^{(+)}\Big), \tag{3}$$

where $q_{j,0}^{(+)} = \sqrt{\vec{q}_j^{\,2}+m_j^2-i0}$ is the positive on-shell energy of the jth line. Then, we iterate the procedure and we get

$$\mathcal{A}_D^{(L)}(1,2,\ldots,k;k+1,\ldots,n) = \sum_{i_k\in k}\mathrm{Res}\Big(\mathcal{A}_D^{(L)}(1,2,\ldots,k-1;k,\ldots,n);q_{i_k,0}^{(+)}\Big), \tag{4}$$

in the kth step. The dual representation for an L-loop amplitude is obtained by computing the Lth iterated residue, and the original scattering amplitude is then written as

$$\mathcal{A}_N^{(L)} = \int_{\vec{\ell}_1\ldots\vec{\ell}_L}\mathcal{A}_D^{(L)}(1,2,\ldots,k;k+1,\ldots,n), \tag{5}$$

with the integration being performed over a Euclidean space (defined by the tensorial product of the space components of the loop momenta) and

$$\int_{\vec{\ell}_i} = \mu^{4-d}\int\frac{d^{d-1}\vec{\ell}_i}{(2\pi)^{d-1}}. \tag{6}$$

It is worth appreciating that several contributions vanished when iterating the residues; these are associated with the so-called displaced poles, which correspond to nonphysical configurations and allow us to define the concept of "nested residues" [23].

Remarkably, further simplifications take place when all the dual contributions (i.e., the terms inside $\mathcal{A}_D^{(L)}$) are explicitly added together: only those terms compatible with causality survive [51]. In fact, Eq. (5) can be recast as

$$\mathcal{A}_N^{(L)} = \sum_{\sigma\in\Sigma}\int_{\vec{\ell}_1\ldots\vec{\ell}_L}(-1)^k\frac{\mathcal{N}_\sigma(\{q_{r,0}^{(+)}\},\{p_{j,0}\})}{x_{L+k}} \times\prod_{i=1}^{k}\frac{1}{\lambda_{\sigma(i)}} + (\sigma\longleftrightarrow\bar{\sigma}), \tag{7}$$

where we introduced the following definitions:

(i) The integration measure, analogous to the real-emission phase space,

$$x_{L+k} = \prod_{j=1}^{L+k}2q_{j,0}^{(+)}. \tag{8}$$

(ii) The order of the topology associated with the Feynman graph $k = V-1$ (with V the number of vertices).

(iii) The causal propagators $1/\lambda_i$, with $\{\lambda_i\}$, are associated with physical threshold singularities of the diagram.

Also, σ represents a combination of "k entangled" physical thresholds from the set Σ of all the compatible thresholds. It turns out that this formulation only contains terms that become singular when going through physical thresholds, manifestly exploiting the underlying causality of QFT and motivating its name: causal dual representation [50,60,61]. It is important to highlight that LTD is "manifestly causal" or, in other words, that such a representation naturally emerges from the principles of the LTD framework [54]. Regarding the set Σ, it can be obtained starting from a purely geometrical formulation [61], similar to the well-known Cutkosky's rules [62].

To conclude this section, let us briefly recall terminology introduced in Refs. [23,50–52]. Given an L-loop scattering amplitude, it belongs to the maximal loop topology (MLT) family if the number of propagators fulfils $n = L+1$. For the next-to-maximal loop topology (NMLT), we have $n = L+2$ and so on. In general, the N^{k}MLT family is composed of L-loop diagrams with $n = L+k+1$ propagators or, equivalently, it is composed of diagrams of topological order k.

III. LTD-INSPIRED STRATEGIES FOR LOCAL RENORMALIZATION

In this section, we describe different strategies to compute local renormalization counterterms. The difference between them lies in the starting point. Whereas the first strategy makes use of the expansion around UV propagators in Minkowski space, the second starts from the LTD causal representation directly.

A. UV expansion in Minkowski space

As already mentioned in the Introduction, given any multiloop, multileg amplitude, the local UV counterterms can be built by Taylor expanding its integrand (depending on the loop four-momenta) in the high-energy limit around the UV propagator, i.e.,

$$G_F(q_{i,\mathrm{UV}}) = \frac{1}{q_{i,\mathrm{UV}}^2 - \mu_{\mathrm{UV}}^2 + i0}, \tag{9}$$

where, for the sake of simplicity, we define $q_{i,\mathrm{UV}} = \ell_i$ and μ_{UV} plays the role of a renormalization scale. The order of the expansion depends on the degree of divergence of the original amplitude in the different UV limits. The procedure is described with plenty of details in Ref. [45], extending previous techniques successfully applied at one-loop level [25,26,44,47].

To illustrate the method, let us first consider the case of the bubble integral in four space-time dimensions, i.e.,

$$\mathcal{A}^{(1)} = \int \frac{d^4k}{(k^2 - m^2)((k-p)^2 - m^2)}, \tag{10}$$

depending on the external four-momentum p. In this case, the superficial degree of divergence is logarithmic (i.e., equal number of powers of the momenta in the numerator and denominator), so the expansion must consider terms of, at least, order $1/|k|^4$. This leads to

$$\begin{aligned}\frac{1}{(k-p)^2 - m^2} = \frac{1}{k^2 - \mu_{\mathrm{UV}}^2}\Bigg\{1 + \frac{2k\cdot p}{k^2 - \mu_{\mathrm{UV}}^2} \\ - \frac{p^2 - m^2 + \mu_{\mathrm{UV}}^2}{k^2 - \mu_{\mathrm{UV}}^2} + \frac{(2k\cdot p)^2}{(k^2 - \mu_{\mathrm{UV}}^2)^2}\Bigg\} \\ + \mathcal{O}\left(\frac{1}{|k|^7}\right),\end{aligned} \tag{11}$$

where subleading terms are also included. Then, the counterterm is written as

$$\begin{aligned}\mathcal{A}_{\mathrm{UV}}^{(1)} = \frac{1}{(k^2 - \mu_{\mathrm{UV}}^2)^2}\Bigg\{1 + \frac{2k\cdot p - p^2}{k^2 - \mu_{\mathrm{UV}}^2} \\ + 2\frac{m^2 - \mu_{\mathrm{UV}}^2}{k^2 - \mu_{\mathrm{UV}}^2}\Bigg\}.\end{aligned} \tag{12}$$

Therefore, the renormalized amplitude $\mathcal{A}_R^{(1)} = \mathcal{A}^{(1)} - \mathcal{A}_{\mathrm{UV}}^{(1)}$ converges, as it goes as $1/|k|^6$ in the UV limit.

The one-loop case is rather simple, since the UV diverging region is well identified, even when working in the Minkowski space (i.e., directly from the Feynman representation). So, as a more refined example, let us consider a two-loop amplitude $\mathcal{A}^{(2)}$, assumed to be free of any IR divergence, and build a set of counterterms that render it integrable in the UV limit. The divergences of the amplitude appear in two different configurations:

(1) when one of the loop four-momenta ℓ_1 or ℓ_2 tend to infinity while the other is fixed (i.e., the so-called simple UV limit),
(2) or when both simultaneously tend to infinity (double UV limit).

Thus, we need to find local counterterms in each of these UV regions. Consequently, the total counterterm $\mathcal{A}_{\mathrm{UV}}^{(2)}$ is given by

$$\mathcal{A}_{\mathrm{UV}}^{(2)} = \mathcal{A}_{\mathrm{UV},1}^{(2)} + \mathcal{A}_{\mathrm{UV},2}^{(2)} + \mathcal{A}_{\mathrm{UV}^2}^{(2)}, \tag{13}$$

where the first two terms on the right-hand side correspond to the simple UV limit, and the last term is obtained from the double UV limit.

In the simple UV limit, $\ell_j \to \infty$, we need first to consider the following replacements:

$$\begin{aligned}S_{\mathrm{UV},j}\colon \{\ell_j^2 | \ell_j\cdot k_i\} \\ \to \{\lambda^2 q_{j,\mathrm{UV}}^2 + (1-\lambda^2)\mu_{\mathrm{UV}}^2 | \lambda q_{j,\mathrm{UV}}\cdot k_i\}.\end{aligned} \tag{14}$$

After the replacements, the expansion in $\lambda \to \infty$ to logarithmic order (denoted by the operator L_λ) allows us to extract the divergent part of the integral. Therefore, the calculation of the counterterm corresponding to the loop four-momentum ℓ_j can be written as

$$\mathcal{A}_{\mathrm{UV},j} = L_\lambda(\mathcal{A}|_{\mathcal{S}_{\mathrm{UV},j}}). \tag{15}$$

It is worth noticing that the highest order in λ depends on the particular expression that we are trying to renormalize: it has to be high enough to cancel all the nonintegrable terms in the UV limit. Still, removing the divergent parts in the individual UV limits is not enough to guarantee integrability: the double UV limit $|\ell_i|, |\ell_j| \to \infty$ has also to be considered to cancel overlapping singularities. The corresponding replacement is

$$\begin{aligned}\mathcal{S}_{\mathrm{UV}^2}\colon \{\ell_j^2 | \ell_j\cdot\ell_k | \ell_j\cdot k_i\} \\ \to \{\lambda^2 q_{j,\mathrm{UV}}^2 + (1-\lambda^2)\mu_{\mathrm{UV}}^2 | \lambda^2 q_{j,\mathrm{UV}}\cdot q_{k,\mathrm{UV}} \\ + (1-\lambda^2)\mu_{\mathrm{UV}}^2/2 | \lambda q_{j,\mathrm{UV}}\cdot k_i\}.\end{aligned} \tag{16}$$

This replacement and the subsequent expansion have to be applied to the original amplitude without the simple UV divergences, namely, $\mathcal{A} - \sum_{k=1}^{L}\mathcal{A}_{\mathrm{UV},k}$. In fact, the simple UV counterterms $\mathcal{A}_{\mathrm{UV},k}$ could be divergent in the double UV limit, so these additional divergences must also be removed by the double limit counterterm. By applying the λ expansion to logarithmic order, we get

$$\mathcal{A}_{\mathrm{UV}^2} = L_\lambda\left(\left(\mathcal{A} - \sum_{j=1,12}\mathcal{A}_{\mathrm{UV},j}\right)\Big|_{\mathcal{S}_{\mathrm{UV}^2}}\right). \tag{17}$$

This strategy can be, in principle, generalized to higher-loop orders. For instance, when the diagram contains three loops, it is necessary to calculate triple limit counterterms. The associated replacement is applied to every different possible combination of loop four-momenta that simultaneously tend to infinity, giving $\binom{L}{3}$ triple counterterms. The replacements and expansion in λ are applied to the original amplitude from which simple and double limit counterterms are already subtracted. That way, the divergences are suppressed in all the possible limits until the integral converges. Still, new overlapping UV-divergent structures might appear, and this procedure could require one to subtract more terms. These potential limitations are the main motivation to explore alternative frameworks.

B. Causal LTD approach

Another way to build local UV counterterms consists of applying the UV expansion directly to the causal dual representation. In this way, the counterterm depends purely on the Euclidean momenta, instead of the four-momenta defined in a Minkowski space. This has several advantages, in particular, working in Euclidean spaces allows a natural definition of distances, so that we can easily associate the high-energy limit with the large loop three-momentum region. Furthermore, the causal dual representation lacks nonphysical singularities in the integrand, which makes the numerical integration of the renormalized amplitude much more stable.

In order to develop this procedure, we start by modifying the algorithm presented in Sec. III A, focusing on promoting scalar products in Minkowski space-time to on-shell energies and scalar products in Euclidean space.

At first order in the expansion $|\vec{\ell}| \to \infty$, the new algorithm transforms the Euclidean space propagator, $1/(\vec{\ell}^2 + m^2)$, into $1/(\vec{\ell}^2 + \mu_{\rm UV}^2)$. Thus, we consider the new replacement rule for the simple UV limit,

$$\begin{aligned} S_{{\rm UV},j}\colon & \left\{\vec{\ell}_j^2 | \vec{\ell}_j \cdot \vec{k}_i\right\} \\ & \to \left\{\lambda^2 \vec{\ell}_j^2 - (1-\lambda^2)\mu_{\rm UV}^2 | \lambda \vec{\ell}_j \cdot \vec{k}_i\right\}, \end{aligned} \tag{18}$$

where $|\vec{\ell}_j| \to \infty$, while $\vec{k}_i$ is kept fixed at a finite value. Notice that the sign in front of the term proportional to $\mu_{\rm UV}^2$ is changed because we are working in a Euclidean space (i.e., we removed the energy component). Regarding the double limit $|\vec{\ell}_j|, |\vec{\ell}_k| \to \infty$, the associated replacement is

$$\begin{aligned} \mathcal{S}_{\rm UV^2}\colon & \left\{\vec{\ell}_j^2 | \vec{\ell}_j \cdot \vec{\ell}_k | \vec{\ell}_j \cdot \vec{k}_i\right\} \\ & \to \Big\{\lambda^2 \vec{\ell}_j^2 - (1-\lambda^2)\mu_{\rm UV}^2 | \\ & \quad \lambda^2 \vec{\ell}_j \cdot \vec{\ell}_k + (1-\lambda^2)\mu_{\rm UV}^2/2 | \lambda \vec{\ell}_j \cdot \vec{k}_i\Big\}. \end{aligned} \tag{19}$$

After implementing Eqs. (18) and (19), the counterterm is defined by expanding the resulting expression in λ around infinity. Analogous replacements could be defined in the simultaneous multiple UV limit, as we will explain later in this section.

At this point, we should notice that there is a crucial detail in this algorithm: the operator L_λ should not be applied to the prefactor $1/x_{L+k}$, because it is related to the integration measure. Let us recall the causal dual representation from Eq. (7), symbolically written as

$$\mathcal{A}_N^{(L)} = \int_{\vec{\ell}_1 \ldots \vec{\ell}_L} \frac{\mathcal{A}_{\rm RED}^{(L)}(\{q_{i,0}^{(+)}\}_{i=1,\ldots,L+k}, \{p_j\}_{j=1,\ldots,N})}{x_{L+k}}, \tag{20}$$

and define the "reduced amplitude" $\mathcal{A}_{\rm RED}^{(L)}$. It is worth mentioning that, while developing this framework, we noticed that Taylor expanding x_{L+k} in the limit $\lambda \to \infty$ leads to spurious divergences that ruined the convergence in the high-energy region (in other words, that prevent the fully local cancellation of UV divergences). Also, we notice that the replacements (18) and (19) can be directly applied at the level of on-shell energies, i.e., $q_{i,0}^{(+)}$, since they transform the three-momenta.

Let us illustrate the proposed technique, considering a generic scalar L-loop scattering amplitude (i.e., the numerator is $\mathcal{N} \equiv 1$). First, we take the UV limit of n-loop three-momenta going simultaneously to infinity; we denote by γ the set of indices corresponding to these loop momenta. Then, let m be the number of internal lines (or propagators) that depend on, at least, one of these n momenta. In this way, scaling the loop three-momenta by λ and doing a naive power counting, we have λ^{3n} in the numerator coming from $\prod_{i\in\gamma} d^3\vec{\ell}_i$ and λ^m in the denominator originated from the integration measure prefactor $1/x_{L+k}$. Thus, in order to define the counterterm in this simultaneous multiple UV limit, $\mathcal{A}_{\rm RED}^{(L)}$ needs to be expanded in λ keeping terms $\mathcal{O}(\lambda^{3n-m})$, besides subleading powers to adjust the finite pieces. For instance, in the case of MLT diagrams [50,53], it would be necessary to expand up to $\mathcal{O}(2n-1)$. For more complicated topologies, such as N^{k}MLT, the superficial degree of UV divergence is lowered both by the prefactor ($x_{L+k} \to \lambda^m$) and the presence of causal entangled thresholds involving several loop momenta going to infinity.

Still, with a larger number of loops, there is a larger number of possible combinations for taking these n simultaneous limits: explicitly, there are $\binom{L}{n}$ multiple UV limits. Therefore, the number of loops significantly increases the complexity of the calculations. Furthermore, overlapping singularities might appear, as in the Minkowski-space expansion, which require keeping higher-order terms in λ. The origin of such singularities is the direct implementation of replacement rules (18) and (19), which could introduce additional spurious dependencies of the loop momenta in the

numerators: this problem is particularly evident at three loops and beyond.

C. On-shell energy expansions within causal LTD

The expansion at the level of the loop three-momenta could lead not only to cumbersome expressions, but also to alter the nice structure of causal LTD representations. Still, if it does not introduce any spurious or noncausal divergence, new functional dependences besides the on-shell energies $q_{i,0}^{(+)}$ will appear.

Let us start with the single UV limit and consider $q_{j,0}^{(+)}$, assuming that it depends on $\vec{\ell}_i$. Using the definition of the on-shell energies and rescaling $\vec{\ell}_i$, we have

$$q_{j,0}^{(+)} = \sqrt{(\vec{\ell}_i + \vec{k})^2 + m_j^2} \to \sqrt{\lambda^2\left(\vec{\ell}_i^{\,2} + \mu_{\rm UV}^2\right) + 2\lambda\vec{\ell}_i\cdot\vec{k} + \vec{k}^2 - \mu_{\rm UV}^2 + m_j^2}, \tag{21}$$

where $\vec{k} \equiv \vec{q}_j - \vec{\ell}_i$. Then, if we expand in λ, we obtain

$$S'_{{\rm UV},i}\colon\ q_{j,0}^{(+)} \to \lambda q_{i,0,{\rm UV}}^{(+)} + \frac{\vec{\ell}_i\cdot\vec{k}}{q_{i,0,{\rm UV}}^{(+)}} - \frac{(\vec{\ell}_i\cdot\vec{k})^2}{2\lambda(q_{i,0,{\rm UV}}^{(+)})^3} + \frac{\vec{k}^2 + m_j^2 - \mu_{\rm UV}^2}{2\lambda q_{i,0,{\rm UV}}^{(+)}} + \mathcal{O}(\lambda^{-2}). \tag{22}$$

If we keep different masses, the replacement in the case $i = j$ with $\vec{k} = 0$ takes the form

$$S'_{{\rm UV},i}\colon\ q_{i,0}^{(+)} \to \lambda q_{i,0,{\rm UV}}^{(+)} + \frac{m_i^2 - \mu_{\rm UV}^2}{2\lambda q_{i,0,{\rm UV}}^{(+)}} + \mathcal{O}(\lambda^{-2}),$$

where the subleading terms depending on $m_i^2 - \mu_{\rm UV}^2$ ensure the local cancellation of UV singularities.

Following these ideas, it is possible to obtain a generalization for describing the multiple UV limit. Let us consider

$$\vec{q}_j = \sum_{k\in\delta}\vec{\ell}_k + \vec{p}_j \tag{23}$$

to be the three-momentum of the jth internal line with mass m_j, where $\vec{p}_j$ is any combination of external momenta and δ_j is the set of indices of the loop momenta on which q_j depends. Let γ be the set of loop three-momenta that are going to infinity and define

$$\vec{\ell}_{j,\gamma} = \sum_{k\in\gamma\cap\delta_j}\vec{\ell}_k, \tag{24}$$

$$\vec{v}_j = \vec{q}_j - \vec{\ell}_{j,\gamma}. \tag{25}$$

With this notation, the replacement from Eq. (19) takes the form

$$q_{j,0}^{(+)} \to \sqrt{\lambda^2(q_{\delta_j\cap\gamma,0,{\rm UV}}^{(+)})^2 + 2\lambda\vec{\ell}_{j,\gamma}\cdot\vec{v}_j + \vec{v}_j^{\,2} - \mu_{\rm UV}^2 + m_j^2}, \tag{26}$$

with $q_{\delta_j\cap\gamma,0,{\rm UV}}^{(+)} = \sqrt{\vec{\ell}_{j,\gamma}^{\,2} + \mu_{\rm UV}^2}$. Notice that this expression is valid regardless of the number of simultaneous divergent loop three-momenta, $\rho = \#(\gamma)$. Then, if we perform a Taylor expansion and keep terms up to $\mathcal{O}(\lambda^{-3})$, the replacement rule $S'_{{\rm UV}^\rho,\gamma}$ simplifies to

$$\begin{aligned} q_{j,0}^{(+)} \to{}& \lambda q_{\delta_j\cap\gamma,0,{\rm UV}}^{(+)} + \frac{\vec{\ell}_{j,\gamma}\cdot\vec{v}_j}{q_{\delta_j\cap\gamma,0,{\rm UV}}^{(+)}} - \frac{(\vec{\ell}_{j,\gamma}\cdot\vec{v}_j)^2}{2\lambda(q_{\delta_j\cap\gamma,0,{\rm UV}}^{(+)})^3} \\ &+ \frac{\vec{v}_j^{\,2} + m_j^2 - \mu_{\rm UV}^2}{2\lambda q_{\delta_j\cap\gamma,0,{\rm UV}}^{(+)}} + \frac{(\vec{\ell}_{j,\gamma}\cdot\vec{v}_j)^3}{2\lambda^2(q_{\delta_j\cap\gamma,0,{\rm UV}}^{(+)})^5} \\ &- \frac{(\vec{\ell}_{j,\gamma}\cdot\vec{v}_j)(\vec{v}_j^{\,2} + m_j^2 - \mu_{\rm UV}^2)}{2\lambda^2(q_{\delta_j\cap\gamma,0,{\rm UV}}^{(+)})^3} \\ &- \frac{5(\vec{\ell}_{j,\gamma}\cdot\vec{v}_j)^4}{8\lambda^3(q_{\delta_j\cap\gamma,0,{\rm UV}}^{(+)})^7} - \frac{(\vec{v}_j^{\,2} + m_j^2 - \mu_{\rm UV}^2)^2}{8\lambda^3(q_{\delta_j\cap\gamma,0,{\rm UV}}^{(+)})^3} \\ &+ \frac{3(\vec{\ell}_{j,\gamma}\cdot\vec{v}_j)^2(\vec{v}_j^{\,2} + m_j^2 - \mu_{\rm UV}^2)}{4\lambda^3(q_{\delta_j\cap\gamma,0,{\rm UV}}^{(+)})^5} + \mathcal{O}(\lambda^{-4}). \end{aligned} \tag{27}$$

At this point, we can define an iterative procedure to locally subtract all the UV-divergent contributions for any arbitrary number of loops. Given an L-loop reduced scattering amplitude $\mathcal{A}_{\rm RED}^{(L)}$, we calculate the simple UV counterterms,

$$\mathcal{A}_{{\rm RED,UV},i_1}^{(L)} = L_\lambda\left(\mathcal{A}_{\rm RED}^{(L)}|_{\mathcal{S}'_{{\rm UV}^1,i_1}}\right), \tag{28}$$

with $i_1 \in \{1,\ldots,L\}$. Then, we subtract the sum of simple UV counterterms to the reduced amplitude, defining

$$\mathcal{A}_{{\rm RED},1}^{(L)} = \mathcal{A}_{{\rm RED},0}^{(L)} - \sum_{i_1=1}^{L}\mathcal{A}_{{\rm RED,UV},i_1}^{(L)}, \tag{29}$$

with $\mathcal{A}_{{\rm RED},0}^{(L)} = \mathcal{A}_{\rm RED}^{(L)}$ to simplify the recursive relations. The next step consists of removing the double UV singularities, which is achieved by defining the double UV counterterms, i.e.,

$$\mathcal{A}_{{\rm RED,UV},\{i_1,i_2\}}^{(L)} = L_\lambda\left(\mathcal{A}_{{\rm RED},1}^{(L)}|_{\mathcal{S}'_{{\rm UV}^2,\{i_1,i_2\}}}\right), \tag{30}$$

and summing them over all the possible couples $\{i_1, i_2\}$. We obtain

$$\mathcal{A}^{(L)}_{\mathrm{RED},2} = \mathcal{A}^{(L)}_{\mathrm{RED},1} - \sum_{i_1=1}^{L} \sum_{i_2=i_1+1}^{L} \mathcal{A}^{(L)}_{\mathrm{RED,UV},i_1 i_2}. \quad (31)$$

Repeating the procedure L times, we arrive to

$$\mathcal{A}^{(L)}_{\mathrm{RED,UV}} = \mathcal{A}^{(L)}_{\mathrm{RED},L-1} - L_\lambda(\mathcal{A}^{(L)}_{\mathrm{RED},L-1}|_{\mathcal{S}'_{\mathrm{UV}^L,\{1,\ldots,L\}}}), \quad (32)$$

which corresponds to the locally renormalized reduced amplitude. Notice that this procedure is rather general, and the operator L_λ could change step by step. This is because L_λ involves performing the λ series expansion to different orders, to ensure that all nonintegrable terms in the limit $\vec{\ell} \to \infty$ are removed. Also, we have to take into account that keeping subleading orders in the first loops might lead to new and more UV singular terms for the remaining loops, implying that the expansion in λ for the subsequent iterations had to be done to higher orders.

To conclude this section, we would like to comment on the loop-momenta flow dependence. Since our approach aims at a local cancellation of the UV divergences, the UV local counterterms could eventually exhibit an *explicit* dependence on the loop momenta. Still, one crucial advantage of the causal LTD representation is that it depends only on on-shell energies, i.e., $q^{(+)}_{i,0}$. So, the loop-momenta dependence is hidden inside these $q^{(+)}_{i,0}$, and any explicit loop-momenta dependence will be generated from the UV expansion of the on-shell energies. In the next section, we will show explicit local UV counterterms, and we will see that their explicit dependence on the loop-momenta flow is minimized.

IV. BENCHMARK MULTILOOP EXAMPLES

In this section, we present representative examples up to three loops and study their numerical convergence. We will rely on the simplified strategy based on on-shell energy expansions. Additionally, we would like to emphasize that our motivation here is limited to show that the UV divergences are canceled with the proposed local renormalization counterterms; being able to provide precise numerical predictions would require high-precision integrators and this study is out of the scope of the present research.

A. Sunrise diagram with equal masses and fixed renormalization scale

A simple diagram that we can use to test our local renormalization strategy is the two-loop MLT sunrise with an external four-momentum $p^\mu = (p_0, \vec{p})$. It is worth mentioning that, in the scalar case (i.e., $\mathcal{N} \equiv 1$), MLT diagrams are the most UV singular (with a superficial degree of divergence $2L - 1$). For the two-loop case, the causal dual representation is given by

$$\mathcal{A}^{(2)} = \int_{\vec{\ell}_1,\vec{\ell}_2} \frac{1}{x_3}\left(\frac{1}{\lambda_1^+} + \frac{1}{\lambda_1^-}\right), \quad (33)$$

where

$$\lambda_1^\pm = q^{(+)}_{1,0} + q^{(+)}_{2,0} + q^{(+)}_{3,0} \pm p_0 \quad (34)$$

are the causal thresholds associated with MLT diagrams and

$$q_1 = \ell_1, \qquad q_2 = \ell_2, \qquad q_3 = \ell_1 + \ell_2 - p \quad (35)$$

is the momenta assignation, as shown in Fig. 1. The corresponding on-shell energies are given by

$$q^{(+)}_{1,0} = \sqrt{\vec{\ell}_1^{\,2} + m_1^2}, \quad (36)$$

$$q^{(+)}_{2,0} = \sqrt{\vec{\ell}_2^{\,2} + m_2^2}, \quad (37)$$

$$q^{(+)}_{3,0} = \sqrt{(\vec{\ell}_1 + \vec{\ell}_2 - \vec{p})^2 + m_3^2}, \quad (38)$$

and we set, in this subsection, $m_1 = m_2 = m_3 = M$ as well as $\vec{p} = \vec{0}$. Therefore, the reduced amplitude is

$$\mathcal{A}^{(2)}_{\mathrm{RED}} = \frac{1}{q^{(+)}_{1,0} + q^{(+)}_{2,0} + q^{(+)}_{3,0} + p_0} + \frac{1}{q^{(+)}_{1,0} + q^{(+)}_{2,0} + q^{(+)}_{3,0} - p_0}. \quad (39)$$

This diagram depends on two-loop momenta $\vec{\ell}_1$ and $\vec{\ell}_2$, so the potential UV-divergent regions to be considered are $|\vec{\ell}_1| \to \infty$ and $|\vec{\ell}_2| \to \infty$, as well as the simultaneous limit $|\vec{\ell}_1|, |\vec{\ell}_2| \to \infty$.

In the case $|\vec{\ell}_1| \to \infty$, Eq. (22) yields the replacement $q^{(+)}_{1,0} \to \lambda q^{(+)}_{1,0,\mathrm{UV}}$ keeping only the leading order in λ, while

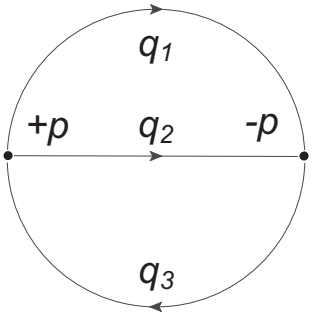

FIG. 1. Momenta assignation for the two-loop MLT diagram studied, according to Eq. (35).

$q_{3,0}^{(+)} \to \lambda q_{1,0,\mathrm{UV}}^{(+)}$ due to the dependence of $\vec{q}_3$ on $\vec{\ell}_1$. After applying these transformations to the reduced amplitude, we get

$$\mathcal{A}^{(2)}_{\mathrm{RED}}|_{S'_{\mathrm{UV},1}} = \frac{1}{2\lambda q_{1,0,\mathrm{UV}}^{(+)} + q_{2,0}^{(+)} + p_0} + \frac{1}{2\lambda q_{1,0,\mathrm{UV}}^{(+)} + q_{2,0}^{(+)} - p_0}, \tag{40}$$

to which the expansion $\lambda \to \infty$ is applied up to order 1, in accordance with the formula found in Sec. II: $3n - 2 = 1$ for $n = 1$ (single UV limit) and $m = 2$ (two other momenta depending on $\vec{\ell}_1$). Finally, the limit $\lambda \to 1$ is taken, and the reduced part of the counterterm is given by

$$\mathcal{A}^{(2)}_{\mathrm{RED,UV},1} = \frac{1}{q_{1,0,\mathrm{UV}}^{(+)}}, \tag{41}$$

meaning that the total counterterm in the limit $|\vec{\ell}_1| \to \infty$ is

$$\mathcal{A}^{(2)}_{\mathrm{UV},1} = \int_{\vec{\ell}_1,\vec{\ell}_2} \frac{1}{x_3 q_{1,0,\mathrm{UV}}^{(+)}}. \tag{42}$$

In the case $|\vec{\ell}_2| \to \infty$, we can exploit the exchange symmetry of the indices $1 \leftrightarrow 2$. This leads directly to the counterterm

$$\mathcal{A}^{(2)}_{\mathrm{UV},2} = \int_{\vec{\ell}_1,\vec{\ell}_2} \frac{1}{x_3 q_{2,0,\mathrm{UV}}^{(+)}}. \tag{43}$$

For the double UV limit, we first define

$$(\mathcal{A}^{(2)}_{\mathrm{RED}})' = \mathcal{A}^{(2)}_{\mathrm{RED}} - \mathcal{A}^{(2)}_{\mathrm{RED,UV},1} - \mathcal{A}^{(2)}_{\mathrm{RED,UV},2}, \tag{44}$$

which corresponds to the original reduced amplitude after subtracting the single UV counterterms. Using Eq. (27), we have

$$q_{1,0}^{(+)} \to \lambda q_{1,0,\mathrm{UV}}^{(+)}, \tag{45}$$

$$q_{2,0}^{(+)} \to \lambda q_{2,0,\mathrm{UV}}^{(+)}, \tag{46}$$

$$q_{3,0}^{(+)} \to \lambda q_{12,0,\mathrm{UV}}^{(+)}, \tag{47}$$

with

$$q_{12,0,\mathrm{UV}}^{(+)} = \sqrt{(\vec{\ell}_1 + \vec{\ell}_2)^2 + \mu_{\mathrm{UV}}^2}, \tag{48}$$

and the condition $\mu_{\mathrm{UV}} \equiv M$. These replacements lead to

$$(\mathcal{A}^{(2)}_{\mathrm{RED}})'|_{S'_{\mathrm{UV}^2}} = \frac{1}{\lambda\left(q_{1,0,\mathrm{UV}}^{(+)} + q_{2,0,\mathrm{UV}}^{(+)} + q_{12,0,\mathrm{UV}}^{(+)}\right) + p_0} + \frac{1}{\lambda\left(q_{1,0,\mathrm{UV}}^{(+)} + q_{2,0,\mathrm{UV}}^{(+)} + q_{12,0,\mathrm{UV}}^{(+)}\right) - p_0}. \tag{49}$$

In this case, the expansion in λ is carried out to order 3. After taking the limit $\lambda \to 1$ and restoring the prefactor, the counterterm of the double UV limit is

$$\mathcal{A}^{(2)}_{\mathrm{UV},12} = \int_{\vec{\ell}_1,\vec{\ell}_2} \frac{1}{x_3}\left(\frac{2p_0^2}{\left(q_{1,0,\mathrm{UV}}^{(+)} + q_{2,0,\mathrm{UV}}^{(+)} + q_{12,0,\mathrm{UV}}^{(+)}\right)^3} + \frac{2}{q_{1,0,\mathrm{UV}}^{(+)} + q_{2,0,\mathrm{UV}}^{(+)} + q_{12,0,\mathrm{UV}}^{(+)}} - \frac{1}{q_{1,0,\mathrm{UV}}^{(+)}} - \frac{1}{q_{2,0,\mathrm{UV}}^{(+)}}\right). \tag{50}$$

Finally, the total counterterm for the sunrise diagram is obtained summing the counterterms for the three limits,

$$\mathcal{A}^{(2)}_{\mathrm{UV}} = \mathcal{A}^{(2)}_{\mathrm{UV},1} + \mathcal{A}^{(2)}_{\mathrm{UV},2} + \mathcal{A}^{(2)}_{\mathrm{UV},12} = \int_{\vec{\ell}_1,\vec{\ell}_2} \frac{2}{x_3}\left(\frac{p_0^2}{Q_{\mathrm{UV}}^3} + \frac{1}{Q_{\mathrm{UV}}}\right), \tag{51}$$

where we defined $Q_{\mathrm{UV}} = q_{1,0,\mathrm{UV}}^{(+)} + q_{2,0,\mathrm{UV}}^{(+)} + q_{12,0,\mathrm{UV}}^{(+)}$, namely, the UV version of the causal threshold present in this MLT diagram. By Taylor expanding, it can be proved that the renormalized amplitude $\mathcal{A}_R^{(2)} = \mathcal{A}^{(2)} - \mathcal{A}^{(2)}_{\mathrm{UV}}$ converges since the divergent orders are exactly canceled in both the simple and the double UV limit.

This example shows the importance of applying the replacement and subsequent Taylor expansion to $(\mathcal{A}^{(2)}_{\mathrm{RED}})'$ instead of $\mathcal{A}^{(2)}_{\mathrm{RED}}$. This is because the simple UV counterterms $\mathcal{A}^{(2)}_{\mathrm{RED,UV},1}$ and $\mathcal{A}^{(2)}_{\mathrm{RED,UV},2}$ add spurious divergences in the double UV limit, which are then subtracted by $\mathcal{A}^{(2)}_{\mathrm{RED,UV},12}$. In this particular example, the counterterms for the simple UV limits are completely eliminated by $\mathcal{A}^{(2)}_{\mathrm{RED,UV},12}$ and they do not appear in the complete UV counterterm. In addition to this, it is important to work with the reduced amplitudes, since the expansion of the prefactor associated with the phase-space measure would introduce additional contributions that prevent a local UV renormalization, unless extra terms are introduced. It is also worth noticing that, in the particular case of $\mathcal{A}^{(2)}_{\mathrm{UV}}$, all the dependencies on the masses and renormalization scale are embodied within the on-shell energies.

Another interesting remark is that the replacements $\mathcal{S}'_{\mathrm{UV}}$, as given in Eqs. (22) and (27) keeping only the leading order in λ, are defined by the Taylor expansion of $\mathcal{S}_{\mathrm{UV}}$ at first order in λ. However, for obtaining the double UV counterterm $\mathcal{A}^{(2)}_{\mathrm{RED,UV},12}$, an expansion in λ up to order 3 is carried out. Therefore, the subleading terms of the original replacement $\mathcal{S}_{\mathrm{UV}^2}$, absent in $\mathcal{S}'_{\mathrm{UV}^2}$, are missing when this new substitution is applied. The convergence of the renormalized amplitude, even without these missing terms

(i.e., just taking into account the leading term of the replacement) is very smooth.

1. Numerical integration

After proving that the renormalized amplitude $\mathcal{A}_R^{(2)}$ is integrable in the UV region by construction, we test the numerical stability of the formalism in $d = 4$ space-time dimensions. For doing so, we use first spherical coordinates to parametrize the loop three-momenta, i.e.,

$$\vec{\ell}_i = \ell_i\{\sin(\theta_i)\cos(\phi), \sin(\theta_i)\sin(\phi), \cos(\theta_i)\}, \quad (52)$$

with $\ell_i \in (0, \infty)$. Then, we compactify the integration domain by changing variables according to

$$\ell_i = \frac{x_i}{1 - x_i}, \quad (53)$$

where $x_i \in (0, 1)$ and the integration measure from Eq. (6) reads

$$\int_{\vec{\ell}_i} = \int_0^1 dx_i \int_0^\pi d\theta_i \int_0^{2\pi} d\phi_i \frac{\sin(\theta_i) x_i^2}{8\pi^3 (1 - x_i)^4}. \quad (54)$$

The UV limit is reached when $x_i \to 1$. Hence, for studying the quality of the convergence of the locally renormalized amplitude, we introduce a cutoff energy Λ such that $\ell_i < \Lambda$ for all the loop three-momenta (in this example, $i = \{1, 2\}$) and numerically evaluated $\mathcal{A}_R^{(2)}$ for different values of Λ. Switching to x_i, this means that the upper limit should set to

$$x_i^{\mathrm{MAX}} = \frac{\Lambda}{1 + \Lambda}. \quad (55)$$

If the cancellation of UV divergences is stable, we expect $\mathcal{A}_R^{(2)}$ to converge as $\Lambda \to \infty$ (or $x_i \to 1$).

In Fig. 2, we present the results for a fully numerical integration of $\mathcal{A}_R^{(2)}$ as a function of the cutoff Λ. We work in arbitrary units, fixing $p_0 = 0.2$ for the external momenta, $M = 0.4$ for the three internal lines, and $\mu_{\mathrm{UV}} = 0.4$ as the renormalization scale. For testing purposes within *Mathematica*, we used four different setups: NIntegrate with *AdaptiveMonteCarlo*, the default NIntegrate, and Cuhre and Vegas from cuba library [63]. The renormalized amplitude increases as higher-energy contributions are taken into account, stabilizing very fast and converging to $\mathcal{A}_R^{(2)} = (372 \pm 2) \times 10^{-6}$. This value is obtained from the average of the integral within the four different scenarios at $\Lambda = 10^{25}$ and leads to a relative error estimation of $\mathcal{O}(1\%)$. Also, we consider the error estimation provided by Vegas, which is fully compatible with the statistical fluctuations among the different integration methods: concretely, it returns $\mathcal{O}(0.4\%)$, on average, over the whole range of Λ.

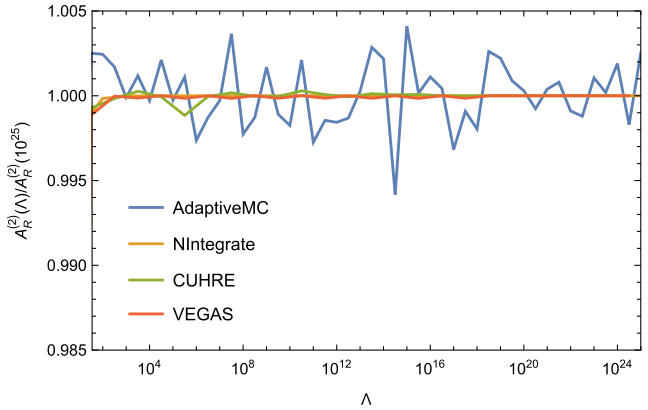

FIG. 2. Analysis of the numerical convergence for the sunrise with equal masses and $\mu_{\mathrm{UV}} = M$, as a function of the cutoff Λ. The results are normalized to $\mathcal{A}_R^{(2)}(\Lambda = 10^{25})$, using $M = 4/10$, $p_0 = 2/10$ and neglecting units. Four different setups are considered for performing the numerical integration, as described in the text.

Finally, we present in Fig. 3 a plot showing the value of the numerical calculation of the renormalized amplitude for different values of M. The cutoff energy was $\Lambda = 10^{25}$ and the energy of the external particle was fixed to $p_0 = 2/10$. We considered different computational setups to test the numerical stability and the smoothness of the mass dependence. In fact, we can see that they are in perfect agreement with each other. For $M > 0.06$, the relative error estimation provided by Vegas is $\mathcal{O}(0.4\%)$ and the relative differences comparing the four different methods is $\mathcal{O}(1.5\%)$. The largest deviations arise in the limit $M \to 0$, where IR singularities appear. In that region, Vegas leads to an error of $\mathcal{O}(15\%–80\%)$ with 500000 integrand evaluations.

B. Generic sunrise diagram

For a generic sunrise diagram, truncating the expansion in λ and retaining only the leading order within the

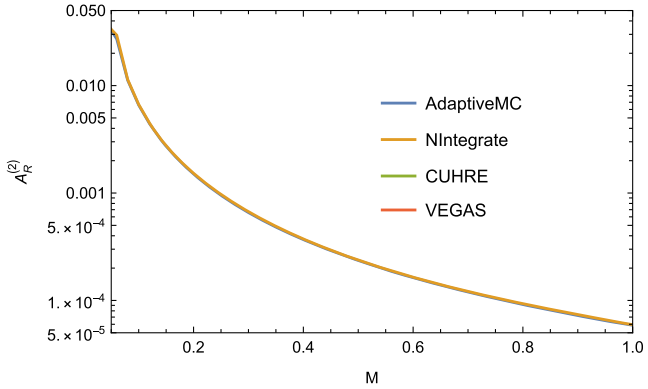

FIG. 3. Analysis of the mass dependence of the renormalized amplitude $\mathcal{A}_R^{(2)}$, with a fixed cutoff $\Lambda = 10^{25}$ and $p_0 = 2/10$. Four different setups are considered for performing the numerical integration, as described in the text.

replacement rules given is not enough to locally cancel the UV divergences. For instance, nontrivial terms involving differences of the masses appear and prevent integrability in the double UV limit. Thus, we need to keep subleading terms in λ within the on-shell energies. If we do so, the total counterterm obtained for the generic sunrise diagram (i.e., a two-loop MLT) is given by

$$\begin{aligned}\mathcal{A}^{(2)}_{\mathrm{UV}} = \int_{\vec{\ell}_1,\vec{\ell}_2} \frac{1}{x_3}\Bigg\{ & \frac{2}{Q_{\mathrm{UV}}} + \frac{1}{Q^2_{\mathrm{UV}}}\Bigg[2\vec{\ell}_{12}\cdot\vec{p} + \frac{m_1^2}{q^{(+)}_{1,0,\mathrm{UV}}} \\ & + \frac{m_2^2}{q^{(+)}_{2,0,\mathrm{UV}}} - \mu^2_{\mathrm{UV}}\left(\frac{1}{q^{(+)}_{1,0,\mathrm{UV}}} + \frac{1}{q^{(+)}_{2,0,\mathrm{UV}}}\right)\Bigg] \\ & + \frac{2p_0^2}{Q^3_{\mathrm{UV}}} + \frac{1}{Q^2_{\mathrm{UV}}(q^{(+)}_{12,0,\mathrm{UV}})^3}\Bigg[\vec{\ell}^{\,2}_{12}(m_3^2+\vec{p}^{\,2}) \\ & - \left(1 + \frac{2q^{(+)}_{12,0,\mathrm{UV}}}{Q_{\mathrm{UV}}}\right)(\vec{\ell}_{12}\cdot\vec{p})^2 - \mu^4_{\mathrm{UV}} \\ & + \mu^2_{\mathrm{UV}}(m_3^2+\vec{p}^{\,2}-\vec{\ell}^{\,2}_{12})\Bigg]\Bigg\}. \end{aligned} \tag{56}$$

Notice that the structure in the numerator is far more complex than the one found in the equal-mass case. Still, if we set $m_i \equiv M$, $\vec{p}=0$ and $\mu_{\mathrm{UV}} = M$, Eq. (56) reduces to Eq. (51). Also, we notice that the explicit loop-momenta flow dependence is rather minimal and only manifests in the numerators: the denominators solely contain combinations of on-shell energies.

Once the counterterm was analytically computed, we proceed to test numerically the quality of the convergence. In the first place, we set $\vec{p}=0$, which is still a rather general case (essentially, this covers any timelike or null vector p^μ when p_0 is real). In Fig. 4, we consider $m_1 = 3/10$, $m_2 = m_3 = 5/10$, $p_0 = 2/10$, and $\mu_{\mathrm{UV}} = 1$, in the four scenarios described in Sec. IV A 1. The renormalized amplitude increases as higher-energy contributions are taken into account, stabilizing very fast and converging to $\mathcal{A}^{(2)}_R = 2.46 \pm 0.09$. This value is obtained from the average of the integral within the four different scenarios at $\Lambda = 10^{25}$. Regarding the error estimation, we obtain a relative error of $\mathcal{O}(7.8\%)$ from the comparison among methods, while VEGAS leads to $\mathcal{O}(0.4\%)$. At this point, we will consider as default estimator during the rest of the work the error provided by VEGAS, since the largest discrepancies come from CUHRE and the default setup of NINTEGRATE. We found that CUHRE largely overestimates the error, leading to $\mathcal{O}(60\%)$, although the difference among the central values with respect to VEGAS is $\mathcal{O}(4\%)$.

Additionally, we test the stability of the numerical results when varying the values of the masses. In particular, as we show in Fig. 5, we keep $m_2 = m_3 = 5/10$, $p_0 = 2/10$, and $\mu_{\mathrm{UV}} = 1$ fixed, and we consider $m_1 \in (1/50, 1)$. The numerical integration was performed using NINTEGRATE

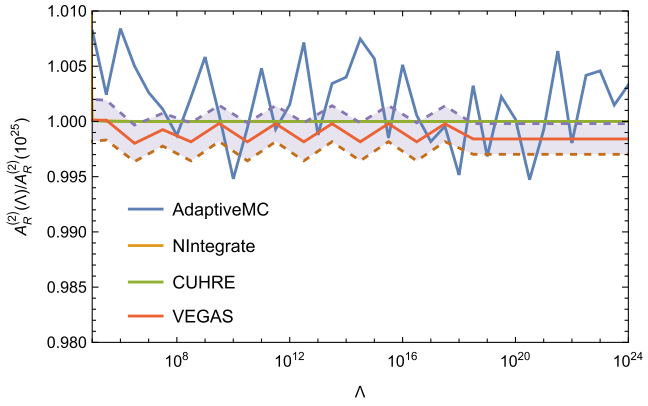

FIG. 4. Analysis of the numerical convergence for the sunrise with different masses, as a function of the cutoff Λ. The results are normalized to $\mathcal{A}^{(2)}_R(\Lambda = 10^{25})$, using $m_1 = 3/10$, $m_2 = m_3 = 5/10$, $\mu_{\mathrm{UV}} = 1$, $p_0 = 2/10$ and neglecting units. Four different setups are considered for performing the numerical integration, as described in the text. The purple error band is generated using the output of VEGAS.

with *AdaptiveMonteCarlo* (blue), the default NINTEGRATE (orange), CUHRE (green), and VEGAS (red). The dependence on m_1 is very smooth, and the error band delimited by the central values obtained with the four methods is $\mathcal{O}(5\%)$ for the low-mass region, although it reaches up to $\mathcal{O}(50\%)$ for $m_1 \approx 1$. We notice that the discrepancies between NINTEGRATE with *AdaptiveMonteCarlo* (blue) and the default NINTEGRATE (orange) are $\mathcal{O}(5\%)$ for the whole range of m_1, and a similar result is obtained when comparing CUHRE (green) and VEGAS (red). Again, CUHRE gives a largely overestimated relative error, while VEGAS with 5000000 points and 10 iterations leads to $\mathcal{O}(0.5\%)$.

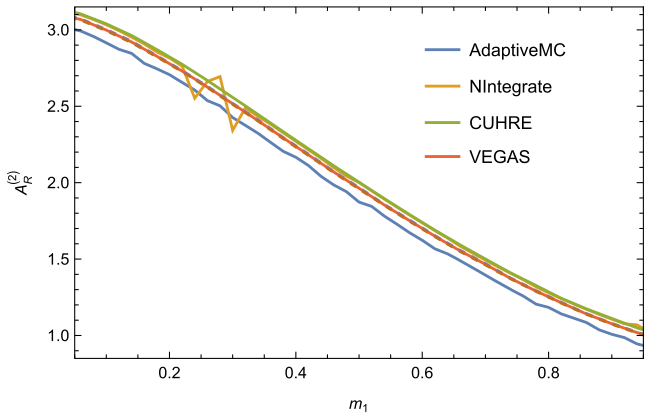

FIG. 5. Analysis of the mass dependence of the renormalized amplitude $\mathcal{A}^{(2)}_R$, with a fixed cutoff $\Lambda = 10^{25}$. We set $m_2 = m_3 = 5/10$, $p_0 = 2/10$, and $\mu_{\mathrm{UV}} = 1$. Three different setups are considered for performing the numerical integration, as described in the text. The error band (purple) is provided by VEGAS, although it can not be appreciated in the plot since it is very small, i.e., $\mathcal{O}(0.5\%)$.

Finally, we study the dependence on the renormalization scale $\mu_{\rm UV}$. For this purpose, we fix $m_1 = 5/10$, $m_3 = 3/10$, and $p_0 = 2/10$ (with $\vec{p} = 0$, as in the previous examples shown in this section). The cutoff scale is set to $\Lambda = 10^{25}$, and we rely on VEGAS with 5000000 points and 10 iterations to integrate the expressions. The relative error provided by this method is $\mathcal{O}(0.8\%)$. In Fig. 6, we vary the value of m_2 within the range $(1/50, 1)$ and consider three different values of $\mu_{\rm UV}$: 1/2 (dashed blue), 1 (red), and 2 (dotted blue). The green region serves as a estimator of the perturbative error associated with $\mathcal{A}_R^{(2)}(\Lambda = 10^{25})$. We observe that the counterterm defined in Eq. (56) successfully cancels, at integrand level, all the UV singular terms for arbitrary values of masses and the renormalization scale.

C. Three-loop MLT diagram

The next step in complexity consists of locally renormalizing a three-loop amplitude. The simplest but most divergent scalar example is the three-loop MLT diagram, given by

$$\mathcal{A}^{(3)} = \int_{\vec{\ell}_1,\vec{\ell}_2,\vec{\ell}_3} \frac{1}{x_4}\left(\frac{1}{\lambda_1^+} + \frac{1}{\lambda_1^-}\right), \tag{57}$$

with

$$\lambda_1^{\pm} = q_{1,0}^{(+)} + q_{2,0}^{(+)} + q_{3,0}^{(+)} + q_{4,0}^{(+)} \pm p_0 \tag{58}$$

the causal threshold, which is totally analogous to the two-loop MLT [50]. The momenta assignation is given by

$$\begin{aligned} &q_1 = \ell_1, \qquad q_2 = \ell_2, \qquad q_3 = \ell_3, \\ &q_4 = \ell_1 + \ell_2 + \ell_3 - p, \end{aligned} \tag{59}$$

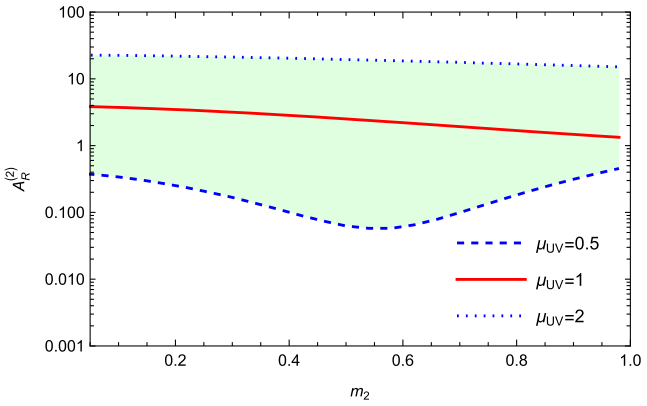

FIG. 6. Analysis of the mass and renormalization scale dependence $\mu_{\rm UV}$ of $\mathcal{A}_R^{(2)}$, with a fixed cutoff $\Lambda = 10^{25}$ and $m_2 \in (1/50, 1)$. The external energy is fixed to $p_0 = 2/10$, as well as $m_1 = 5/10$ and $m_3 = 3/10$. We use the VEGAS method to perform the numerical integration.

and the on-shell energies are

$$q_{1,0}^{(+)} = \sqrt{\vec{\ell}_1^{\,2} + m_1^2}, \tag{60}$$

$$q_{2,0}^{(+)} = \sqrt{\vec{\ell}_2^{\,2} + m_2^2}, \tag{61}$$

$$q_{3,0}^{(+)} = \sqrt{\vec{\ell}_3^{\,2} + m_3^2}, \tag{62}$$

$$q_{4,0}^{(+)} = \sqrt{(\vec{\ell}_1 + \vec{\ell}_2 + \vec{\ell}_3 - \vec{p})^2 + m_4^2}. \tag{63}$$

Then, the reduced amplitude is obtained from the integrand of Eq. (57) by removing the prefactor $1/x_4$. The procedure for computing the local counterterm is analogous to the one described for the generic sunrise, although the intermediate step expressions are more lengthy. First, we need to compute the single UV counterterms for $|\vec{\ell}_i| \to \infty$ for $i = \{1, 2, 3\}$, expanding the reduced amplitude in λ and retaining up to $\mathcal{O}(\lambda^{-1})$ terms: these are equivalent to Eq. (41). Then, the double UV counterterms require to expand up to $\mathcal{O}(\lambda^{-3})$, while the triple UV counterterms up to $\mathcal{O}(\lambda^{-5})$. For the sake of completeness, the final counterterm is provided as a publicly available Zenodo file [64].

After deriving the counterterm, we proceed to test the numerical cancellation of nonintegrable contributions in all the UV limits. The locally renormalized amplitude behaves as $1/|\vec{\ell}|^4$, $1/|\vec{\ell}|^7$, and $1/|\vec{\ell}|^{10}$ in the single, double, and triple UV limits, respectively: this implies that it is integrable in the whole UV region.

Following with the tests, we study the convergence of the numerical integration for increasing values of the UV cutoff. After setting $\vec{p} = 0$, we consider $m_1 = 4/10$, $m_2 = m_3 = m_4 = 6/10$, $p_0 = 2/10$, and $\mu_{\rm UV} = 1$, using two different methods within NINTEGRATE: *AdaptiveMonteCarlo* (blue line) and default configuration (orange line). For this particular case, even if the local cancellation of UV singularities is guaranteed, the numerical precision required to converge in a reasonable amount of time exceeds the limit of double precision available within CUBA library. Thus, in this subsection, we rely only on NINTEGRATE since it allows one to perform the calculations with more than 100 digits of precision. The results are shown in Fig. 7. The relative error associated with NINTEGRATE with *AdaptiveMonteCarlo* is $\mathcal{O}(2\%$–$5\%)$, using 1×10^6 points, while the default configuration provides an overestimation of $\mathcal{O}(100\%)$: in any case, both methods lead to compatible results within the error bands. The renormalized amplitude tends to stabilize very fast, already reaching the asymptotic value for $\Lambda = 10^5$ with the default NINTEGRATE method. Still, MonteCarlo based methods tends to oscillate more and the convergence occurs within a band of $\mathcal{O}(10\%)$. By averaging over these two methods, the renormalized amplitude is

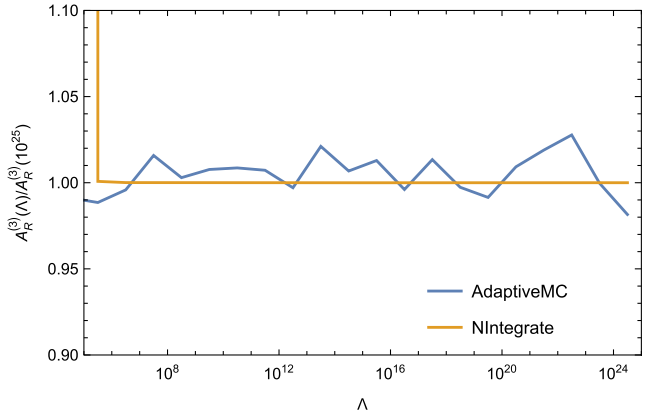

FIG. 7. Analysis of the numerical convergence for the three-loop MLT diagram with different masses, as a function of the cutoff Λ. The results are normalized to $\mathcal{A}_R^{(3)}(\Lambda = 10^{25})$, using $m_1 = 4/10$, $m_2 = m_3 = m_4 = 6/10$, $\mu_{\rm UV} = 1$, $p_0 = 2/10$ and neglecting units.

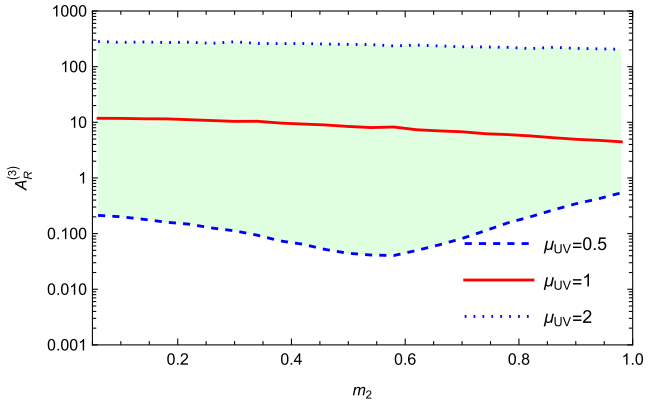

FIG. 9. Analysis of the mass and renormalization scale dependence $\mu_{\rm UV}$ of $\mathcal{A}_R^{(3)}$, with a fixed cutoff $\Lambda = 10^{25}$ and $m_2 \in (1/50, 1)$. The external energy is fixed to $p_0 = 2/10$, as well as $m_1 = 5/10$ and $m_3 = m_4 = 3/10$. We use NIntegrate with the *AdaptiveMonteCarlo* method to perform the numerical integration.

$\mathcal{A}_R^{(3)}(\Lambda = 10^{25}) = 3.5 \pm 1.3$. Notice that the error is larger than the one found for the generic sunrise diagram; this could be further reduced by increasing the number of evaluations within the integrators.

Again, we test the stability of the numerical results when varying the values of the masses. In particular, as we show in Fig. 8, we keep $m_2 = m_3 = 5/10$, $p_0 = 2/10$, and $\mu_{\rm UV} = 1$ fixed. We consider $m_1 \in (1/48, 1)$ and three different scenarios: $m_4 = m_2/2$ (blue), $m_4 = m_2$ (orange), and $m_4 = 2m_2$ (green). The numerical integration was performed using NIntegrate with *AdaptiveMonteCarlo*. We tested other numerical integrators, but they were less efficient in converging. As we saw in the two-loop MLT case, the dependence on m_1 is very smooth, as well as the transition for different values of m_4. Furthermore, the results follow the expected behavior: the heavier the particles, the less probable their production or their presence within the loop.

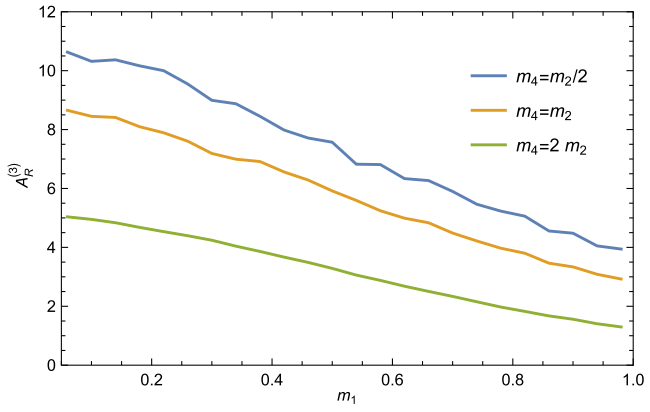

FIG. 8. Analysis of the mass dependence of the renormalized amplitude $\mathcal{A}_R^{(3)}$, with a fixed cutoff $\Lambda = 10^{25}$. We set $m_2 = m_3 = 5/10$, $p_0 = 2/10$, and $\mu_{\rm UV} = 1$. Then, we vary $m_1 \in (1/48, 1)$ and consider three different values of m_4: $m_4 = m_2/2$ (blue), $m_4 = m_2$ (orange), and $m_4 = 2m_2$ (green).

To conclude, we study the dependence on the renormalization scale $\mu_{\rm UV}$. We fix $m_1 = 5/10$, $m_3 = m_4 = 3/10$, and $p_0 = 2/10$ (with $\vec{p} = 0$), together with $\Lambda = 10^{25}$. In Fig. 9, we vary the value of m_2 within the range $(1/48, 1)$, and consider three different values of $\mu_{\rm UV}$: 1/2 (dashed blue), 1 (red), and 2 (dotted blue). As expected, the local counterterm cancels all the UV singular terms for arbitrary values of masses and the renormalization scale. Still, we can appreciate that the dependence on $\mu_{\rm UV}$ is very strong: the results change roughly 2 orders of magnitude when modifying the scale by a factor 2 up or down. This suggests a very strong divergent behavior in the UV, pointing to the correctness of the proposed local counterterms (i.e., if they were wrong, the result would diverge wildly).

D. Three-loop NMLT diagram

The final benchmark example reported in this work is a three-loop NMLT diagram without any external momenta (i.e., a vacuum diagram). The corresponding reduced amplitude is given by

$$\mathcal{A}_{\rm RED}^{(3)} = \frac{1}{\lambda_1\lambda_2} + \frac{1}{\lambda_2\lambda_3} + \frac{1}{\lambda_3\lambda_1}, \tag{64}$$

where

$$\lambda_1 = q_{1,0}^{(+)} + q_{2,0}^{(+)} + q_{3,0}^{(+)} + q_{4,0}^{(+)}, \tag{65}$$

$$\lambda_2 = q_{1,0}^{(+)} + q_{2,0}^{(+)} + q_{5,0}^{(+)}, \tag{66}$$

$$\lambda_3 = q_{3,0}^{(+)} + q_{4,0}^{(+)} + q_{5,0}^{(+)} \tag{67}$$

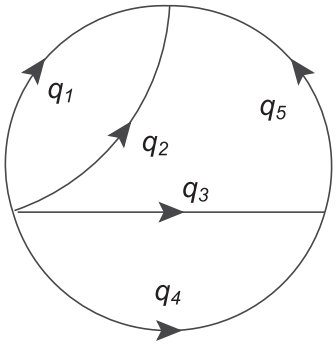

FIG. 10. Momenta assignation for the three-loop NMLT diagram according to Eq. (68).

are the causal thresholds associated with the vacuum NMLT topology and

$$q_1 = \ell_1, \qquad q_2 = \ell_2, \qquad q_3 = \ell_3,$$
$$q_4 = -\ell_1 - \ell_2 - \ell_3, \qquad q_5 = -\ell_1 - \ell_2 \tag{68}$$

are the momenta assignation, as shown in Fig. 10. The explicit expression of the on-shell energies is given by

$$q_{1,0}^{(+)} = \sqrt{\vec{\ell}_1^{\,2} + m_1^2}, \tag{69}$$

$$q_{2,0}^{(+)} = \sqrt{\vec{\ell}_2^{\,2} + m_2^2}, \tag{70}$$

$$q_{3,0}^{(+)} = \sqrt{\vec{\ell}_3^{\,2} + m_3^2}, \tag{71}$$

$$q_{4,0}^{(+)} = \sqrt{(\vec{\ell}_1 + \vec{\ell}_2 + \vec{\ell}_3)^2 + m_4^2}, \tag{72}$$

$$q_{5,0}^{(+)} = \sqrt{(\vec{\ell}_1 + \vec{\ell}_2)^2 + m_5^2}. \tag{73}$$

In order to build the counterterm, we start looking at the single UV limit. As we explained before, the expansion in λ has to be done up to order $3n - m$ around infinity, with m number of internal lines depending on the n-divergent loop three-momenta $\vec{\ell}_\gamma$. Hence, we set $n = 1$ for the single UV limit. For the momenta $\vec{\ell}_1$ and $\vec{\ell}_2$, we have $m = 3$ and the amplitude is already integrable in the limits $|\vec{\ell}_1| \to \infty$ and $|\vec{\ell}_2| \to \infty$. However, for $\vec{\ell}_3$, it is $m = 2$, so we need to expand the reduced amplitude up to order 1. Then, the corresponding local counterterm for the reduced amplitude is given by

$$\mathcal{A}^{(3)}_{\mathrm{RED,UV},3} = \frac{1}{q_{3,0,\mathrm{UV}}^{(+)}\left(q_{1,0}^{(+)} + q_{2,0}^{(+)} + q_{5,0}^{(+)}\right)} = \frac{1}{q_{3,0,\mathrm{UV}}^{(+)}\lambda_2}, \tag{74}$$

which leaves unchanged the causal threshold associated with λ_2.

Regarding the double UV limit ($n = 2$), there are three cases. All of them have $m = 4$, i.e., four propagators depend on $\{\ell_i, \ell_j\}$ for any pair i, j. Then, the expansion is carried out up to order $3n - m = 2$ in λ. After applying the replacement rule $S'_{\mathrm{UV}^\rho,\gamma}$ (with $\rho = 2$ and $\gamma = \{\{1,2\},\{1,3\},\{2,3\}\}$) defined in Eq. (27) to

$$(\mathcal{A}^{(3)}_{\mathrm{RED}})' = \mathcal{A}^{(3)}_{\mathrm{RED}} - \mathcal{A}^{(3)}_{\mathrm{RED,UV},3}, \tag{75}$$

and expanding up to order 2 in λ, we obtain

$$\mathcal{A}^{(3)}_{\mathrm{RED,UV},12} = \frac{1}{Q_{2,\mathrm{UV}}}\left(\frac{1}{q_{12,0,\mathrm{UV}}^{(+)}} - \frac{1}{q_{3,0,\mathrm{UV}}^{(+)}}\right) + \frac{1}{Q_{2,\mathrm{UV}}^2}, \tag{76}$$

$$\mathcal{A}^{(3)}_{\mathrm{RED,UV},13} = \frac{1}{q_{1,0,\mathrm{UV}}^{(+)}}\left(\frac{1}{\tilde{Q}_{13,\mathrm{UV}}} - \frac{1}{2q_{3,0,\mathrm{UV}}^{(+)}}\right) + \frac{1}{\tilde{Q}_{13,\mathrm{UV}}^2}, \tag{77}$$

$$\mathcal{A}^{(3)}_{\mathrm{RED,UV},23} = \frac{1}{q_{2,0,\mathrm{UV}}^{(+)}}\left(\frac{1}{\tilde{Q}_{23,\mathrm{UV}}} - \frac{1}{2q_{3,0,\mathrm{UV}}^{(+)}}\right) + \frac{1}{\tilde{Q}_{23,\mathrm{UV}}^2}, \tag{78}$$

where we introduced the shorthand notation

$$\tilde{Q}_{ij,\mathrm{UV}} = q_{i,0,\mathrm{UV}}^{(+)} + q_{j,0,\mathrm{UV}}^{(+)} + q_{ij,0,\mathrm{UV}}^{(+)}, \tag{79}$$

and $Q_{2\mathrm{UV}}$ corresponds to the UV version of the causal threshold λ_2, i.e.,

$$Q_{2,\mathrm{UV}} = q_{1,0,\mathrm{UV}}^{(+)} + q_{2,0,\mathrm{UV}}^{(+)} + q_{12,0,\mathrm{UV}}^{(+)}. \tag{80}$$

Notice that $\tilde{Q}_{ij,\mathrm{UV}}$ is not directly related to a causal threshold of the original Feynman diagram.

Finally, in the triple UV limit, we start from the reduced amplitude without the simple and double UV counterterms, i.e.,

$$(\mathcal{A}^{(3)}_{\mathrm{RED}})'' = (\mathcal{A}^{(3)}_{\mathrm{RED}})' - \mathcal{A}^{(3)}_{\mathrm{RED,UV},12} - \mathcal{A}^{(3)}_{\mathrm{RED,UV},13} - \mathcal{A}^{(3)}_{\mathrm{RED,UV},23}, \tag{81}$$

and perform the expansion in λ up to order 4. This is because $n = 3$ (three simultaneous momenta are going to infinity) and $m = 5$ (there are five internal lines). The resulting counterterm is lengthy, thus we present it as a publicly available file in Zenodo [64].

As in the other examples, we tested the convergence. In the first place, we verify that the renormalized amplitude is integrable in the whole UV region, since it behaves as $1/|\vec{\ell}|^4$, $1/|\vec{\ell}|^7$, and $1/|\vec{\ell}|^{11}$ in the single, double, and triple UV limits, respectively. Furthermore, we check that it behaves as $1/|\vec{\ell}|^5$ when only $|\vec{\ell}_1| \to \infty |\vec{\ell}_2| \to \infty$, pointing toward a faster convergence.

After that, we analyze the convergence, varying the UV cutoff. In Fig. 11, we set $m_1 = 4/10$, $m_2 = m_3 = m_4 = 1/10$, $m_5 = 4/10$, and $\mu_{\rm UV} = 1$, using three different methods: NIntegrate with *AdaptiveMonteCarlo* (blue line), the default NIntegrate (orange line), and Vegas (red line). The renormalized amplitude quickly reaches the asymptotic value, although oscillations are present (as in the three-loop MLT case). By averaging over these three methods, the renormalized amplitude is $\mathcal{A}_R^{(3)}(\Lambda = 10^{25}) = 35 \pm 13$, which leads to a relative error of $\mathcal{O}(70\%)$. Still, the individual methods have large errors: $\mathcal{O}(100\%)$ for the default NIntegrate scenario and $\mathcal{O}(20\%)$ for Vegas (orange band). The estimation for NIntegrate with *AdaptiveMonteCarlo* is $\mathcal{O}(1\%)$, using 5×10^6 points, and the method converges much faster than the other two strategies: for this reason, we set it as default for the next studies of this section.

The next check consisted of studying the stability of the integral when varying the values of the masses. In Fig. 12, we keep $m_2 = m_3 = 4/10$, $m_5 = 3/10$, and $\mu_{\rm UV} = 1$ fixed. We consider $m_1 \in (1/48, 1)$ and three different scenarios: $m_4 = m_2/2$ (blue), $m_4 = m_2$ (orange), and $m_4 = 2m_2$ (green). The dependence on both m_1 and m_4 is smooth, and the value of the integral decreases when heavier particles are considered. Again, this confirms the overall good quality of the local UV cancellation.

Finally, we examine the dependence on the renormalization scale $\mu_{\rm UV}$. We keep fixed $m_1 = 2/10$, $m_3 = m_4 = 3/10$, and $m_5 = 1/10$, and the cutoff $\Lambda = 10^{25}$. Then, we vary m_2 within the range $(1/48, 1)$, as we show in Fig. 13. We consider three different values of $\mu_{\rm UV}$: $1/2$ (dashed blue), 1 (red), and 2 (dotted blue). The band formed around the central value (i.e., for $\mu_{\rm UV} = 1$) is very wide, covering roughly 2 orders of magnitude. Again, this indicates that the original integral is very UV divergent and that the local counterterms found with our procedure successfully neutralize these nonintegrable terms.

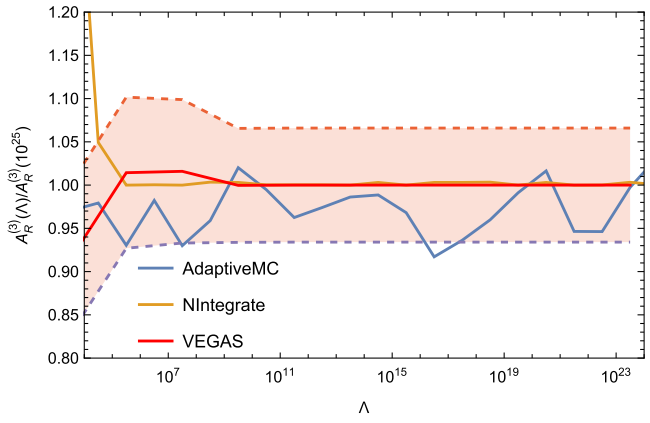

FIG. 11. Analysis of the numerical convergence for the three-loop NMLT diagram with different masses, as a function of the cutoff Λ. The results are normalized to $\mathcal{A}_R^{(3)}(\Lambda = 10^{25})$, using $m_1 = 4/10$, $m_2 = m_3 = m_4 = 1/10$, $m_5 = 4/10$, $\mu_{\rm UV} = 1$ and neglecting units. The orange error band is obtained using Vegas.

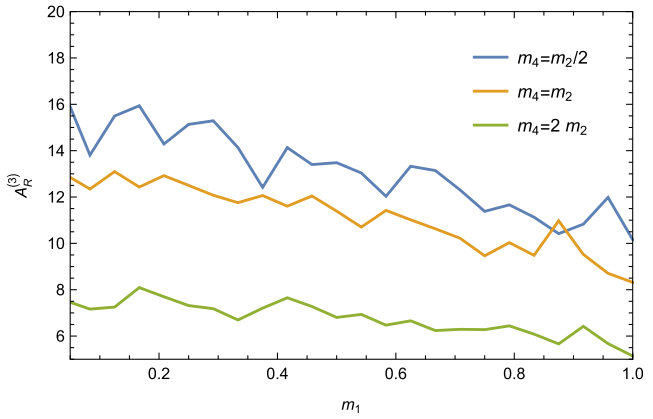

FIG. 12. Analysis of the mass dependence of the renormalized amplitude $\mathcal{A}_R^{(3)}$, with a fixed cutoff $\Lambda = 10^{25}$. We set $m_2 = m_3 = 4/10$, $m_5 = 3/10$, and $\mu_{\rm UV} = 1$. Then, we vary $m_1 \in (1/48, 1)$ and consider three different values of m_4: $m_4 = m_2/2$ (blue), $m_4 = m_2$ (orange), and $m_4 = 2m_2$ (green).

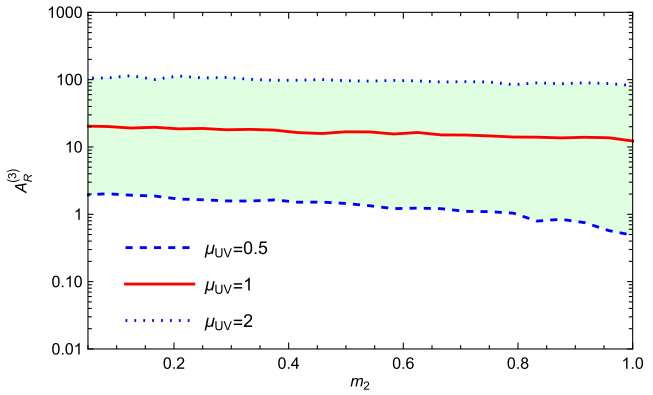

FIG. 13. Analysis of the mass and renormalization scale dependence $\mu_{\rm UV}$ of $\mathcal{A}_R^{(3)}$, with a fixed cutoff $\Lambda = 10^{25}$ and $m_2 \in (1/48, 1)$. We fix $m_1 = 2/10$, $m_3 = m_4 = 3/10$, and $m_5 = 1/10$.

V. CONNECTION TO BPHZ APPROACH

As stated in the Introduction, techniques for getting rid of UV singularities are well established in the literature. One relevant example in the context of this work is the Bogoliubov-Parasiuk-Hepp-Zimmermann formalism. It was originally developed by Bogoliubov and Parasiuk in Ref. [34] and consisted of the definition of an operator

acting on diagrams with the purpose of locally removing the UV singularities. This operator, known as Bogoliubov's R operator, relies on Taylor-like expansions in momentum space combined with graph theory techniques to identify overlapping singularities. It was shown that this strategy can successfully remove UV singularities for any renormalizable QFT [37], even at higher perturbative orders. Recently, there were efforts to define an extended operator, the R^* operator [65], capable of removing both IR and UV singularities.

The purpose of this section is to compare the BPHZ approach with respect to the local renormalization program within causal loop-tree duality. As a first step, let us consider a graph Γ. Then, the BPHZ R operator acting on Γ is given by

$$R_\gamma \equiv 1 - t_p^{\delta(\Gamma)}. \tag{82}$$

The operator $t_p^{\delta(\Gamma)}$ symbolizes the Taylor expansion up to order $\delta(\Gamma)$ (the UV degree of divergence of the graph or subgraph), depending on the external momenta p, that extracts the divergent part of the diagram. It is important to notice that this Taylor expansion is equivalent to the expansion around the UV propagator described in Sec. III A (as shown in the Appendix): the operator t_p is analogous to L_λ in our formalism, choosing $\mu_{\rm UV} = m$.

Also, we observe that taking the UV limit of a set of loop momenta δ corresponds to the application of the R operator to a certain subdiagram whose internal lines only depend on the loop momenta $\ell_i \in \delta$. In particular, the R operator applied on the whole graph Γ is equivalent to the simultaneous UV limit of all loop momenta. Thus, we appreciate a parallelism with the operators $\mathcal{S}'_{{\rm UV},i}$ introduced in Sec. III B to take the simultaneous UV limit of i-loop momenta.

Additionally, to discuss the removal of divergences of each subgraph $\gamma \in \Gamma$, let us write the decomposition

$$I_\Gamma(p,k) = I_{\Gamma/\gamma} I_\gamma(p^\gamma, k^\gamma), \tag{83}$$

where contracting γ to a point within Γ leads to the "reduced diagram" Γ/γ. The external momenta k^γ and p^γ have to be chosen consistently with the parametrization of Γ and the energy-momentum conservation at the vertices. Then, the UV-expansion operator t_γ applied to the amplitude I_Γ, removes the subdivergence coming from γ.

Once we identify common aspects of both strategies, we proceed to look into more detail the different operations performed. On one hand, the first step of our UV-expansion algorithm consists of removing the single UV limits. Using the notation introduced for BPHZ formalism, the single UV counterterm can be rewritten as

$$\mathcal{A}^{(L)}_{{\rm RED},1} = \left(1 - \sum_{i=1} t_{\gamma_i}\right) \mathcal{A}^{(L)}_{{\rm RED},0}. \tag{84}$$

Then, the counterterms for the double UV limit take the form

$$\mathcal{A}^{(L)}_{{\rm RED},2} = \left(1 - \sum_{k=1}^{L-1} \sum_{j>k}^{L} t_{\gamma_{jk}}\right)\left(1 - \sum_{i=1}^{L} t_{\gamma_i}\right) \mathcal{A}^{(L)}_{{\rm RED},0}. \tag{85}$$

Finally, iterating the procedure, the locally renormalized amplitude is given by

$$\mathcal{A}^{(L)}_{{\rm RED},L} = \prod_{l=1}^{n}\left(1 - \sum_{i=\{i_1,\ldots,i_n\}} t_{\gamma_{\{i_1,\ldots,i_n\}}}\right) \mathcal{A}^{(L)}_{{\rm RED},0}, \tag{86}$$

where the summation is carried out over all ordered pairs $\{i_1, \ldots, i_n\}$.

On the other hand, let us consider Zimmermann's forest formula [37], i.e.,

$$R_\Gamma I_\Gamma = (1 - t_\Gamma) \sum_\alpha \left(\prod_{\gamma \in \mathcal{F}_\alpha} (-t_\gamma)\right) I_\Gamma. \tag{87}$$

Now, let us consider a graph without disjoint subgraphs, meaning that a couple of subgraphs can just be nonoverlapping if one of the subgraphs is contained in the other. It was shown by Bergere and Zuber [66] that the product of t_γ operators of overlapping graphs applied on an amplitude is zero. So, it follows that Zimmermann's forest formula (87) has the same form of Eq. (86). In the case that the diagram considered has disjoint subgraphs, the algorithm presented in this paper would need to be modified to recover Zimmermann's forest formula. In fact, in Eq. (86), there are some missing terms where the divergences of disjoint subgraphs are simultaneously removed, unlike in Eq. (87).

To end this comparison between both strategies, it should be noted that all the calculations and reasoning in this section are equally valid when working in three-dimensional Euclidean space. Therefore, the local renormalization proposed in this article by means of UV expansions within causal loop-tree duality is equivalent to the BPHZ approach, in the case of Feynman diagrams without disjoint subgraphs. Still, since our local renormalization technique starts from the causal LTD representation, it has the advantage that the structure of the denominators is independent of the explicit momenta labeling: only on-shell energies appear (which, of course, implicitly depends on the momenta configuration).

VI. CONCLUSIONS AND OUTLOOK

In this work, we explored techniques for achieving an integrand-level renormalization of multiloop, multileg scattering amplitudes. We started by reviewing a method

that exploits the expansion of the integrand around the UV propagator in the Minkowski space. Even if this technology was successfully tested in Refs. [25,26,45,47] up to two loops, going beyond this level poses additional difficulties. These difficulties are mainly related to the presence of new overlapped singularities introduced by counterterms in the different UV limits. In this regard, we also showed that our method shares several nice properties with the BPHZ renormalization program, in particular, when dealing with graphs without disjoint subgraphs.

Thus, we exploited the nice properties of loop-tree duality [14] to perform the UV expansion in a Euclidean space. We took advantage of the so-called causal dual representations [50] to expand around the infinite three-momentum regions inside the positive on-shell energies, which leads to more compact expressions. We tested the methodology with scalar Feynman integrals belonging to the maximal loop topology family at two and three loops and the next-to-maximal loop topology at three loops. In all the cases, the counterterms found locally cancel the non-integrable terms of the original amplitude in all the UV limits, hence rendering the expressions integrable in four space-time dimensions and without the need of introducing any additional regularization method.

One key aspect of the formalism presented in this work is the definition of reduced amplitudes and the subsequent application of the UV expansion on them, instead of acting on the whole amplitude. In this way, the local renormalization does not alter the integration measure that appears in the causal dual representation; any multiloop, multileg renormalized scattering amplitude reads

$$\mathcal{A}^{(L)}_{R,N} = \int_{\vec{\ell}_1 \ldots \vec{\ell}_L} \sum_k \frac{1}{x_{L+k}} (\mathcal{A}^{(L,k)}_{\mathrm{RED}} - \mathcal{A}^{(L,k)}_{\mathrm{RED,UV}}), \quad (88)$$

where we are summing over different topological families of order k. This will be particularly relevant in the context of the FDU [24–26] approach, since the dual (i.e., virtual after the application of LTD) contribution is combined, at integrand level, with the real radiation. This real-dual combination involves a kinematical mapping, and keeping a phase-space measure within the contributions coming from loops plays a crucial role in the local cancellation of IR divergences. Thus, in sight of a unified framework to compute physical observables at higher order directly in four space-time dimensions [67,68], our findings regarding local renormalization from causal LTD might be very helpful.

Supporting data for this paper are openly available from the Zenodo repository [64].

ACKNOWLEDGMENTS

We would like to thank Germán Rodrigo, Roger Hernández-Pinto, and Leandro Cieri for the fruitful discussion about loop-tree duality and for providing us very useful comments about the manuscript. This work was supported by the Spanish Government (Agencia Estatal de Investigación MCIN/AEI/ 10.13039/501100011033) Grants No. PID2019–105439GB-C22, No. PID2020–114473GB-I00, and No. PID2022-141910NB-I00 and Generalitat Valenciana Grants No. PROMETEO/2021/071 and No. ASFAE2022/009. G. S. is partially supported by EU Horizon 2020 research and innovation program STRONG-2020 project under Grant Agreement No. 824093 and H2020-MSCA-COFUND USAL4EXCELLENCE-PROOPI-391 project under Grant Agreement No. 101034371.

APPENDIX: EQUIVALENCE OF MOMENTUM EXPANSIONS IN THE UV LIMIT

In order to show the equivalence between the expansion around the UV propagator (as described in Sec. III A) and BPHZ renormalization in Minkowski space-time, let us consider a propagator depending on an arbitrary number of loop and external momenta. Let us define the propagator of the jth internal line as

$$\Delta(k_j, m_j) = \frac{1}{k_j^2 - m_j^2}, \quad (A1)$$

where $k_j = \sum_{n\in\delta_j} \ell_n + \sum_i p_i$. δ_j is the set of indices of loop momenta ℓ on which the jth internal four-momentum depends. The summation over i also runs through all external momenta on which it depends. Let us consider the UV limit of some loop momenta, whose indices define the set γ. Applying the replacements given in Eqs. (14)–(16) (depending whether it is a simple or multiple UV limit) and setting $\mu_{\mathrm{UV}} = m_j$, the propagator in Eq. (A1) becomes

$$\begin{aligned}
&\Delta(k_j, m_j)|_{\mathcal{S}_{\mathrm{UV},\gamma}} \\
&= \frac{1}{\left(\lambda \sum_{\substack{n\in\delta_j \\ n\in\gamma}} \ell_n + \sum_{\substack{m\in\delta_j \\ m\notin\gamma}} \ell_m + \sum_i p_i\right)^2 - \lambda^2 m_j^2} \\
&= \frac{x^2}{\left(\sum_{\substack{n\in\delta_j \\ n\in\gamma}} \ell_n + x\left(\sum_{\substack{m\in\delta_j \\ m\notin\gamma}} \ell_m + \sum_i p_i\right)\right)^2 - m_j^2}
\end{aligned} \quad (A2)$$

where the replacement $x = \frac{1}{\lambda}$ is carried out. This way, a Taylor expansion at $\lambda \to \infty$ corresponds to expanding x around 0. After this expansion, the final result is recovered by taking the limit $x \to 1$.

On the other hand, it can be shown by a change of variables that

$$x^n \frac{d^n}{dx^n} = \left(\sum_{\substack{m\in\delta_j \\ m\notin\gamma}} l_m \frac{\partial}{\partial l_m} + \sum_i p_i \frac{\partial}{\partial p_i}\right)^n. \quad (A3)$$

Then, the Taylor expansion of the propagator up to order N can be obtained from

$$\sum_{n=0}^{N}\frac{1}{n!}\left(\sum_{\substack{m\in\delta_j\\ m\notin\gamma}} l_m\frac{\partial}{\partial l_m}+\sum_i p_i\frac{\partial}{\partial p_i}\right)^n\Delta(k_j,m_j). \tag{A4}$$

Let us now define $\overline{p_i}$, which can be an external momentum or a loop momentum that does not belong to γ. In other words, the momenta labeled by $\overline{p_i}$ are kept finite. Then, we can write

$$\begin{aligned}\left(\sum_{\substack{m\in\delta_j\\ m\notin\gamma}} l_m\frac{\partial}{\partial l_m}+\sum_i p_i\frac{\partial}{\partial p_i}\right)^n\Delta(k_j,m_j) &= \left(\sum_i \bar{p}_i\frac{\partial}{\partial \bar{p}_i}-\sum_{s\notin\delta_j} l_s\frac{\partial}{\partial l_m}\right)^n\Delta(k_j,m_j)\\ &= \left(\sum_i \bar{p}_i\frac{\partial}{\partial \bar{p}_i}\right)^n\Delta(k_j,m_j)=\bar{p}^{\mu_1}_{i_1}\cdots\bar{p}^{\mu_l}_{i_l}\frac{\partial^l\Delta(k_j,m_j)}{\partial\bar{p}^{\mu_1}_{i_1}\cdots\partial\bar{p}^{\mu_l}_{i_l}}.\end{aligned} \tag{A5}$$

Therefore, it is shown that the UV-expansion algorithm proposed in Sec. III taking $\mu_{\rm UV}=m$ and applied on a single propagator corresponds exactly to the Taylor expansion performed within the Bogoliubov's R operation in the BPHZ formalism. The argument presented here can be straightforwardly generalized to deal with an amplitude with an arbitrary number of propagators.

[1] G. Heinrich, Phys. Rep. **922**, 1 (2021).
[2] G. 't Hooft and M. J. G. Veltman, Nucl. Phys. **B44**, 189 (1972).
[3] J. C. Collins, *Renormalization*, Cambridge Monographs on Mathematical Physics Vol. 26 (Cambridge University Press, Cambridge, England, 2023).
[4] We refer the interested reader to Refs. [32,33] for updated, although not fully complete, reviews on the topic.
[5] C. G. Bollini and J. J. Giambiagi, Nuovo Cimento B **12**, 20 (1972).
[6] J. F. Ashmore, Lett. Nuovo Cimento **4**, 289 (1972).
[7] G. M. Cicuta and E. Montaldi, Lett. Nuovo Cimento **4**, 329 (1972).
[8] T. Kinoshita, J. Math. Phys. (N.Y.) **3**, 650 (1962).
[9] For instance, see Ref. [69] and references therein.
[10] C. Anastasiou and G. Sterman, J. High Energy Phys. 07 (2019) 056.
[11] C. Anastasiou, R. Haindl, G. Sterman, Z. Yang, and M. Zeng, J. High Energy Phys. 04 (2021) 222.
[12] C. Anastasiou and G. Sterman, J. High Energy Phys. 05 (2023) 242.
[13] G. Sterman and A. Venkata, J. High Energy Phys. 02 (2024) 101.
[14] S. Catani, T. Gleisberg, F. Krauss, G. Rodrigo, and J.-C. Winter, J. High Energy Phys. 09 (2008) 065.
[15] I. Bierenbaum, S. Catani, P. Draggiotis, and G. Rodrigo, J. High Energy Phys. 10 (**2010**) 073.
[16] I. Bierenbaum, S. Buchta, P. Draggiotis, I. Malamos, and G. Rodrigo, J. High Energy Phys. 03 (2013) 025.
[17] S. Buchta, G. Chachamis, P. Draggiotis, I. Malamos, and G. Rodrigo, J. High Energy Phys. 11 (2014) 014.
[18] S. Buchta, G. Chachamis, P. Draggiotis, and G. Rodrigo, Eur. Phys. J. C **77**, 274 (2017).
[19] J. Plenter, Acta Phys. Pol. B **50**, 1983 (2019).
[20] J. Plenter and G. Rodrigo, Eur. Phys. J. C **81**, 320 (2021).
[21] J. Plenter, Asymptotic expansions and causal representations through the loop-tree duality, Ph.D. thesis, Valencia Univ., IFIC, 2022.
[22] R. Runkel, Z. Szőr, J. P. Vesga, and S. Weinzierl, Phys. Rev. D **101**, 116014 (2020).
[23] J. Aguilera-Verdugo *et al.*, Symmetry **13**, 1029 (2021).
[24] R. J. Hernandez-Pinto, G. F. R. Sborlini, and G. Rodrigo, J. High Energy Phys. 02 (**2016**) 044.
[25] G. F. R. Sborlini, F. Driencourt-Mangin, R. Hernandez-Pinto, and G. Rodrigo, J. High Energy Phys. 08 (2016) 160.
[26] G. F. R. Sborlini, F. Driencourt-Mangin, and G. Rodrigo, J. High Energy Phys. 10 (**2016**) 162.
[27] R. M. Prisco and F. Tramontano, J. High Energy Phys. 06 (2021) 089.
[28] R. Pittau, J. High Energy Phys. 11 (2012) 151.
[29] A. M. Donati and R. Pittau, Eur. Phys. J. C **74**, 2864 (2014).
[30] R. Pittau, Fortschr. Phys. **63**, 601 (2015).
[31] B. Page and R. Pittau, J. High Energy Phys. 11 (2015) 183.
[32] C. Gnendiger *et al.*, Eur. Phys. J. C **77**, 471 (2017).
[33] W. J. Torres Bobadilla *et al.*, Eur. Phys. J. C **81**, 250 (2021).
[34] N. N. Bogoliubov and O. S. Parasiuk, Acta Math. **97**, 227 (1957).
[35] K. Hepp, Commun. Math. Phys. **2**, 301 (1966).
[36] W. Zimmermann, Commun. Math. Phys. **6**, 161 (1967).
[37] W. Zimmermann, Commun. Math. Phys. **15**, 208 (1969).
[38] J. H. Lowenstein and W. Zimmermann, Nucl. Phys. **B86**, 77 (1975).

[39] M. Gomes, J. H. Lowenstein, and W. Zimmermann, Commun. Math. Phys. **39**, 81 (1974).
[40] J. H. Lowenstein and W. Zimmermann, Commun. Math. Phys. **44**, 73 (1975).
[41] J. H. Lowenstein, Commun. Math. Phys. **47**, 53 (1976).
[42] J. H. Lowenstein, in *International School of Mathematical Physics, 2nd Course: Renormalization Theory* (1975).
[43] D. N. Blaschke, F. Gieres, F. Heindl, M. Schweda, and M. Wohlgenannt, Eur. Phys. J. C **73**, 2566 (2013).
[44] S. Becker, C. Reuschle, and S. Weinzierl, J. High Energy Phys. 12 (2010) 013.
[45] F. Driencourt-Mangin, G. Rodrigo, G. F. R. Sborlini, and W. J. Torres Bobadilla, J. High Energy Phys. 02 (2019) 143.
[46] F. Driencourt-Mangin, Four-dimensional representation of scattering amplitudes and physical observables through the application of the loop-tree duality theorem, Ph.D. thesis, Univ. Valencia (main), 2019, arXiv:1907.12450.
[47] F. Driencourt-Mangin, G. Rodrigo, G. F. R. Sborlini, and W. J. Torres Bobadilla, Phys. Rev. D **105**, 016012 (2022).
[48] E. Tomboulis, J. High Energy Phys. 05 (2017) 148.
[49] J. J. Aguilera-Verdugo, F. Driencourt-Mangin, J. Plenter, S. Ramírez-Uribe, G. Rodrigo, G. F. R. Sborlini, W. J. Torres Bobadilla, and S. Tracz, J. High Energy Phys. 12 (2019) 163.
[50] J. J. Aguilera-Verdugo, F. Driencourt-Mangin, R. J. Hernandez Pinto, J. Plenter, S. Ramirez-Uribe, A. E. Renteria Olivo, G. Rodrigo, G. F. Sborlini, W. J. Torres Bobadilla, and S. Tracz, Phys. Rev. Lett. **124**, 211602 (2020).
[51] J. J. Aguilera-Verdugo, R. J. Hernandez-Pinto, G. Rodrigo, G. F. R. Sborlini, and W. J. Torres Bobadilla, J. High Energy Phys. 01 (2021) 069.
[52] S. Ramírez-Uribe, R. J. Hernández-Pinto, G. Rodrigo, G. F. R. Sborlini, and W. J. Torres Bobadilla, J. High Energy Phys. 04 (2021) 129.
[53] J. Aguilera-Verdugo, R. J. Hernández-Pinto, G. Rodrigo, G. F. R. Sborlini, and W. J. Torres Bobadilla, J. High Energy Phys. 02 (2021) 112.
[54] J. Aguilera-Verdugo, R. J. Hernández-Pinto, S. Ramírez-Uribe, G. Rodrigo, G. F. R. Sborlini, and W. J. Torres Bobadilla, in *Snowmass 2021—Letter of Intention* (2020).
[55] R. Runkel, Z. Szőr, J. P. Vesga, and S. Weinzierl, Phys. Rev. Lett. **122**, 111603 (2019); **123**, 059902(E) (2019).
[56] Z. Capatti, V. Hirschi, D. Kermanschah, and B. Ruijl, Phys. Rev. Lett. **123**, 151602 (2019).
[57] Z. Capatti, V. Hirschi, D. Kermanschah, A. Pelloni, and B. Ruijl, arXiv:2009.05509.
[58] G. Rodrigo, S. Catani, T. Gleisberg, F. Krauss, and J.-C. Winter, Nucl. Phys. B, Proc. Suppl. **183**, 262 (2008).
[59] R. P. Feynman, Acta Phys. Pol. **24**, 697 (1963).
[60] W. J. Torres Bobadilla, J. High Energy Phys. 04 (2021) 183.
[61] G. F. R. Sborlini, Phys. Rev. D **104**, 036014 (2021).
[62] R. E. Cutkosky, J. Math. Phys. (N.Y.) **1**, 429 (1960).
[63] T. Hahn, Comput. Phys. Commun. **168**, 78 (2005).
[64] J. Rios-Sanchez and G. Sborlini, Ancillary files for "Toward multiloop local renormalization within causal loop-tree duality," Zenodo, 10.5281/zenodo.10692163 (2024).
[65] F. Herzog and B. Ruijl, J. High Energy Phys. 05 (2017) 037.
[66] M. C. Bergere and J. B. Zuber, Commun. Math. Phys. **35**, 113 (1974).
[67] S. Ramírez-Uribe, P. K. Dhani, G. F. R. Sborlini, and G. Rodrigo, arXiv:2404.05491.
[68] S. Ramírez-Uribe, A. E. Rentería-Olivo, D. F. Rentería-Estrada, J. J. M. de Lejarza, P. K. Dhani, L. Cieri, R. J. Hernández-Pinto, G. F. R. Sborlini, W. J. Torres Bobadilla, and G. Rodrigo (LTD Collaboration), arXiv:2404.05492.
[69] J. Baglio, C. Duhr, B. Mistlberger, and R. Szafron, J. High Energy Phys. 12 (2022) 066.